Doctoral Dissertation

First-principles Study of Interfacial Interactions between Carbon Nanotube and Ceramics Surfaces for Composite Materials

Irfan Dwi Aditya

July 2018

Division of Precision Science and Technology and Applied Physics
Graduate School of Engineering
Osaka University

Abstract

Ceramic-based materials have been widely used in industrial application at high temperatures due to their excellent mechanical strength, intrinsic thermal stability, and low density. However, ceramics are known to exhibit low fracture toughness since plastic deformation in ceramics is very limited. The toughness of nanoceramics can be enhanced by adding second phase reinforcements such as carbon nanotube (CNT) which has excellent mechanical properties. Until now, however, most results for strengthening and toughening have been disappointing due to the lack of knowledge about the nature of the interface. This dissertation aims to elucidate the nature of the interaction between CNT and the surface of the ceramic. The influences by change of CNT diameter and by stoichiometry of the ceramic surface to the interaction were especially examined, which have never been discussed before.

Our results show that the interfacial interaction between CNT and ceramic surfaces depends greatly on the diameter of CNT. As the diameter increases, the interaction between the CNT and the ceramic surface weakens. It is also highly dependent on the stoichiometry of the ceramic surface. The adhesive energy of the interaction between CNTs and non-stoichiometric ceramic surfaces are negatively larger than the case when CNT interacts with stoichiometric surfaces. Therefore, the CNT with a smaller diameter largely contributes the high performance on the mechanical properties of fracture toughness as well as the strength when it interacts with the nonstoichiometric ceramic surface.

Fracture toughness, which is most expected to be improved by the CNT-composite, also depends on the interface property. The strong interface can resist the crack propagation which might be dependent on the adhesive energy and also the covalent/ionic character of the interface if it is assumed that the large covalent character affects the possibility of bond trapping of cracks.

Contents

List of Tables

TABLE 5. 1 Properties comparison of several ceramic materials[1] 44
TABLE 5. 2 Mechanical properties of CNT-SiC composites by Ma[20] and CNT-Si_3N_4 composites Balaszi[21]. 45
TABLE 5. 3 Comparison of the unit vectors *a*, *b* and *c* of Bulk SiC calculation with reference[25] 47

List of Figures

Chapter 1 Introduction

1.1 Overview

The development of advanced technologies in many sectors requires high performance materials with good mechanical properties, very high thermal conductivity and good wear resistance. Ceramic-based materials such as zirconia (ZrO_2), alumina (Al_2O_3), silicon carbide (SiC), have been widely used in industrial application at high temperatures due to their excellent mechanical strength, intrinsic thermal stability, and low density. However, ceramics are known to exhibit low fracture toughness since plastic deformation in ceramics is very limited. Several approaches have been used to increase the fracture toughness of ceramics material. These include transformation toughening, ductile-phase toughening and reinforcement toughening[1].

In the past few years, considerable attention has been paid to the development of nanocrystalline ceramics with improved mechanical strength and stiffness, and enhanced wear resistance[2-4]. Decreasing the grain size of ceramics to the submicrometer/nanometer scale leads to a marked increase in hardness and fracture strength. However, nanocrystalline ceramics generally display worse fracture toughness than their microcrystalline counterparts[2]. The toughness of nanoceramics can be enhanced by adding second phase reinforcements.

Carbon nanotubes (CNTs) with high aspect ratio, extraordinary mechanical strength and stiffness, excellent thermal and electrical conductivity are attractive nanofillers which produce high-performance ceramic composites with multifunctional properties. The reinforcing effect of CNTs with high aspect ratio is considered to be analogous to that of continuous or short-fiber-reinforcement. The superior flexibility of CNTs is very effective in improving the fracture toughness of brittle ceramics. This is accomplished by means of crack deflection at the CNT–matrix interface, crack-bridging and CNT pull-out mechanisms. Recently, Huang et al. reported that SWNTs exhibit superplastic deformation with an apparent elongation of 280% at high temperatures[5]. This result shows the potential application of CNTs as a toughening element for ceramic matrix composites (CMCs) with improved ductility. Thus, such ceramic-CNT nanocomposite could possess superplastic deformability.

They indicated that superplastic forming of nanocomposites is made easier by adding CNTs[6]. All these attractive and unique properties of CNTs enable materials scientists to create novel strong and tough ceramic nanocomposites. Moreover, the electrical and thermal conductivities of ceramics can be improved markedly by adding nanotubes. On the other hand, experimental results shows that the Young modulus and Ultimate Tensile Stress decreases with increasing CNT diameter which means it violates the rule of mixture on fibre reinforced composite.[7]

Until now, however, most results for strengthening and toughening have been disappointing, and only little or no improvement have been reported in CNT-ceramic composite materials. The problem that now occurs is how to unite CNT with ceramic material because it is very difficult to unify these two materials. Equally important is to control the interface between the CNT and the ceramic to obtain the desired new material properties. For example, to increase the fracture toughness of the ceramics, a

less strong bond between the CNT and the ceramic surface is required. Meanwhile, to increase the elasticity of ceramics, strong bonding between CNT and ceramic surface is required. Furthermore, good interfacial bonding is required to achieve load transfer across the CNT-matrix interface, a condition necessary for improving the mechanical properties of ceramic composites.

Recently, Yamamoto et al has succeeded in making alumina composite by using CNT to increase its mechanical properties. They performed a fibre pullout test on the CNT and found a very strong bond between the CNT and the alumina indicated by the "sword-in-sheath" fracture mode[8]. Other studies also show that the as-produced Al_2O_3 should be a mixture of the rich types of amorphous nanostructure and for the rich types of amorphous structures, the surface curvature of CNT could also play a certain role due to the various possibilities of interface between metal oxide and CNT[9].

So far, several factors have been found that influence the interfacial interaction between CNT and ceramics, such as the diameter of the CNT and the surface of the ceramic itself. The experimental results show that the Young modulus and ultimate tensile stress of the CNT based composite decreases with increasing CNT diameter[7] meanwhile the results of other studies show that stoichiometry of the ceramic surface plays an important role in the interaction between ceramics with other materials[10]. However, the nature of the interaction between CNTs and ceramics and their effects on these factors are unknown.

1.2 Research Objectives

Based on the information described above, it needs to understand the properties of the interface and its role in controlling fracture, it is essential to know the

mechanisms of adhesion at the interface involved. This dissertation aims to elucidate the nature of the interaction of the interaction between CNT and the surface of the ceramic. In addition, in this dissertation will also be examined on the influence of CNT diameter and stoichiometry of the ceramic surface to the interaction.

1.3 Outline of Dissertation

The rest of this dissertation consist of six parts. In chapter 2 we briefly explain the background related to this research, such as explanation about fibre reinforced composites, previous results on CNT based composites, and experimental and computational results of the CNT-ceramics composites.

In chapter 3, we focuse on structural properties of CNTs from density functional theory calculations. The great interest in one-dimensional nanostructures such as nanotubes and nanowires is partly driven by the possibility of being used as strengthening material in nanosized composites and the effect of CNTs diameter on the physical properties of zigzag CNTs deserves to be understood in detail. We present a comparative study of lattice parameters, atomic structures and cohesive energies of zigzag SWCNTs with different diameters.

In Chapter 4, we focus on the interfacial interaction between CNT and Al_2O_3. The CNT diameter dependence and surface termination of Al_2O_3 surface on interfacial interaction between CNT and Al_2O_3 are discussed here.

In Chapter 5, we discuss the interaction between CNT and SiC surfaces. SiC is chosen because experiments show that it has a strong bond with CNT and also because

SiC is non-oxide ceramics, making it interesting for discussion because it will have different interaction characteristics with CNT as compared to Al_2O_3.

In chapter 6 we discuss about the interaction between CNT and ZrO_2 surfaces. ZrO_2 is chosen because, although both are oxide ceramics such as Al_2O_3, but both of them have different stoichiometric surfaces which make it has a different interactions with CNTs.

References

1. S. Zhang, D. Sun, Y. Fu, and H. Du, Surf. Coat.Tech., 198, 2–8. (2005).
2. R.S. Mishra, C.E. Lesher, and A.K. Mukherjee, J.. Am. Ceram. Soc., 79, 2989–2992. (1996).
3. G.D. Zhan, J. Kuntz, J. Wan, J. Garay, and A.K. Mukherjee, Scrip. Mat., 47, 737–741. (2002).
4. B.N. Kim, K. Hiraga, K. Morita, and H. Yoshida, Scrip. Mat., 57, 607–610. (2007).
5. J.Y. Huang, S. Chen, Z.Q. Wang, K. Kempa, Y.M. Wang, S.H. Jo, G. Chen, M.S. Dresselhaus, and Z.F. Ren, Nature, 439, 281. (2006).
6. A. Peigney, F. Flahaut, C. Laurent, F. Chastel, and A. Rousset, Chem. Phys.Lett., Elsevier. vol. 352, pp. 20-25. (2002)
7. Y Sun, and Q Chen; Appl. Phys. Lett. **95**, 021901 (2009); doi: 10.1063/1.3168520
8. G. Yamamoto, M. Omori, T. Hashida, H. Kimura, Nano.. 19, 315708 (2008).
9. Z. Lan, X. Zhang, H. Zhang, X. Ye, *and* X. Zhang, J. App. Phys. **122**, 175104 (2017).
10. H. Li, L.Chen, X. Yuan, W. Zhang, J. R. Smith, A. G. Evans, J. Am. Ceram. Soc., 94 [S1] S154–S159 (2011).

Chapter 2 Backgrounds and Computational Details

2.1 Carbon Nanotubes

In composite materials, where two different materials are combined together for reinforcement, the opportunity exists to design composites for specific properties at various levels of scale. At the microscopic level, we control the fiber orientation, type, and volume fraction to get the desired local stiffness, strength, toughness and other properties of composite material. Recent advances in producing nanostructured materials with novel material properties have stimulated research to create macroscopic engineering materials by designing the structure at the nanoscale through experiment and simulation.

Since their observation in 1991 by lijima[1], carbon nanotubes have been the focus of considerable research. At the nanometer scale, carbon nanotubes show exceptional mechanical and physical properties with predicted elastic moduli of about 1 TPa (1000 GPa), strengths in the range of 50 GPa, and exceptional resilience, showing large nonlinear elastic deformation before fracture. With potential applications ranging from molecular electronics and field-emission displays to nanocomposites, carbon nanotubes offer tremendous opportunity in the development of nanotechnologies.

As scientists and engineers seek to make practical materials and devices from nanostructures, understanding material behavior across length scales from the atomistic to macroscopic levels is required. Knowledge of how the nanoscale structure influences

the nanotube properties as well as how nanotubes interact when embedded in a composite is needed to realize the potential for carbon nanotubes as reinforcement in composites. The change in reinforcement scale from microns of traditional fiber reinforcements to nanometers poses fundamentally new challenges in the processing, characterization and modeling of these materials.

In traditional fiber-reinforced based composites, we need to understand the properties of the constituent materials first and then we combine the materials to examine the synergy. Unlike traditional fibers, obvious difficulties are encountered in testing nanotubes to investigate the stiffness, statistical strength, and transport properties with experimental techniques of their size. Therefore an approach other than experimental studies is needed, one of the most popular methods to do is to use computational studies.

Carbon nanotubes are cylindrical substances comprising only carbon atoms with a diameter smaller than the wavelength of visible light (~400–800 μm), they cannot be observed directly by an optical microscope and so must be observed under electron microscopes. The bonds between carbon atoms that form hexagonal shapes such as benzene rings, known as "sp^2 carbons", are the strongest of all atomic bonds. A carbon nanotube consists entirely of this strongest bond, and therefore, it is extremely resistant to the mechanical load.

The single- and multi-wall nanotubes are interesting nanoscale materials for the following four reasons:

1. Single- and multi-wall nanotubes have very good elastic mechanical properties which derive from two-dimensional (2D) arrangement of carbon atoms in a graphene sheet allows large out-of-plane distortions, while very strong C-C bonds keeps the graphene sheet exceptionally strong against any in-plane distortion or fracture. These structural and material characteristics of nanotubes point towards their possible use in making next generation of extremely lightweight, but highly elastic, and very strong composite materials.
2. A single-wall nanotube can be either conducting or semiconducting, depending on its chiral vector *(n, m),* where n and m are two integers. The rule is that when the difference *n-m* is a multiple of three, a conducting nanotube is obtained. If the difference is not a multiple of three, a semiconducting nanotube is obtained. In

addition, it is also possible to connect nanotubes with different chiralities creating nanotube hetero-junctions, which can form a variety of nanoscale molecular electronic device components.

3. Nanotubes, by structure, are high aspect-ratio objects with good electronic and mechanical properties. Consequently, the applications of nanotubes in field-emission displays or scanning probe microscopic tips for metrological purposes, have started to materialize even in the commercial sector.
4. Since nanotubes are hollow, tubular, caged molecules, they have been proposed as lightweight large surface area packing material for gas-storage and hydrocarbon fuel storage devices, and gas or liquid filtration devices, as well as nanoscale containers for molecular drug-delivery and casting structures for making nanowires and nanocapsulates.

The excellent mechanical properties of nanotubes include an extremely high Young's modulus and tensile strength. Based on previous studies, Young's modulus of nanotubes is in the order of 1 TPa, and its tensile strength is 50 GPa or higher. Since both these values are several times higher than those of steel and its specific gravity is less than one-tenth that of steel, it offers 100 times larger mechanical strength than steel with the same weight. In fact, nanotubes are so robust that by weaving them into a fiber, Theoretically, it would be possible to hang a weight of 1200 tons from a rope just 1 cm in diameter. Thus, it is far stronger than any existing materials.

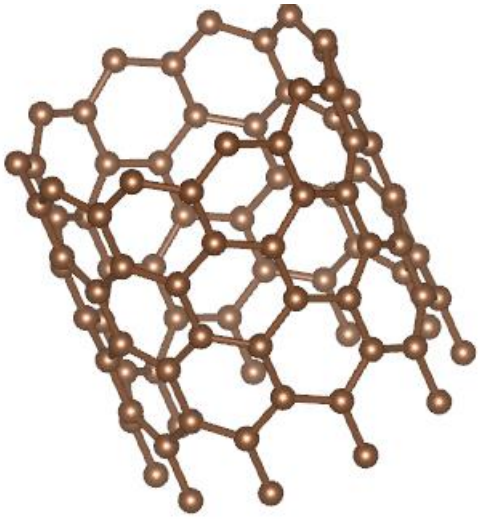

FIG. 2. 1 Schematic diagrams of carbon nanotubes

2.2 CNT Based Composite

The development of advanced technologies in the electronics, aerospace and energy sectors requires materials with excellent mechanical properties, high thermal conductivity and good wear resistance. Due to the various advantages that have been mentioned in the previous section, CNT is widely used as a reinforcing material on composites. Several studies have discussed the use of CNTs as reinforcement in composites, both experimental and computational studies.

A lot of research work on CNT composites has concentrated to improved electrical conductivity, optical devices, and higher strength [2-4]. For example, CNT are used to improve the mechanical properties and the heat deflection temperatures of carbon nanotube/ poly (vinyl alcohol) composites[5] and carbon nanotube/ poly (methyl methacrylate) composites[6] both prepared by direct mixing were raised with the increase of the content of CNTs. Kuzumaki et al.[7] prove that the mechanical properties of the composites were more thermally stable than that of pure Al by characterize the processing and mechanical properties of carbon nanotube-reinforced aluminum composites prepared by hotpressing.

However, there are only few studies carried out on CNT-reinforced ceramic matrix composites. Peigney et al.[8-11] developed techniques to synthesize carbon nanotubes/metal-oxide composite powders. He processes this powders using hot-press to obtain composites. The result, however, did not provide the expected improvement in mechanical properties.

Chang et al.[12] fabricated alumina matrix composites containing 5-20 volume percent of multiwall carbon nanotubes. This mixture produces improvement of 24% on fracture toughness compared with that of the single phase alumina. Ma et al.[13] produces

carbon nanotube/SiC composite powder by using mixing nanosize SiC particles with 10% carbon nanotubes and then hot pressing it. the results of his research showed an increase in both the strength and the fracture toughness by 10% as compared to the monolithic ceramics.

The effective utilization of nanotubes in composite applications depends strongly on the ability to disperse CNTs homogeneously throughout the matrix. Furthermore, good interfacial bonding is required to achieve load transfer across the CNT-matrix interface, a condition necessary for improving the mechanical properties.

Experimental results of carbon nanotube (CNT) reinforced copper composites (Cu/CNT) have shown that the resultant tensile strength of Cu/CNT composite depends on CNT diameter, in a form of parabolic relationship that the smaller CNT diameters result in greater total interfacial bonding area thus the greater resultant strength of the composite as depicted in FIG 2.2. This results also shows that the Young modulus and Ultimate Tensile Stress decreases with increasing CNT diameter[14].

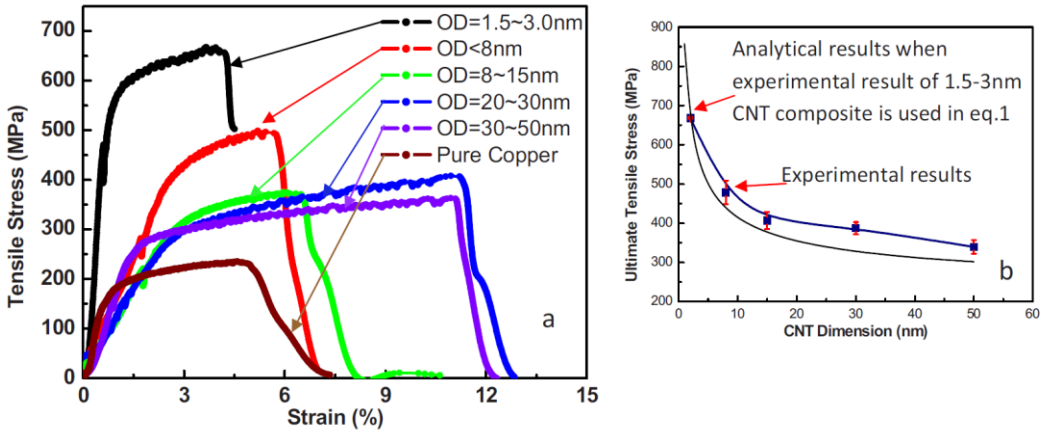

FIG. 2. 2 Color online a Tensile stress-strain curve of pure Cu and Cu/CNT composites with different diameters and averaged tensile strengths versus CNT diameters of Cu/CNT composites (Figure 4 of Ref.14).

2.3 CNT-Ceramic Composite

Ceramic-based materials such as alumina (Al_2O_3), zirconia (ZrO_2), and silicon carbide (SiC) are good candidates to be used in such applications due to their intrinsic thermal stability, good corrosion resistance, high temperature mechanical strength and low density. However, ceramics are known to exhibit extreme brittle nature and low fracture toughness since plastic deformation in ceramics is very limited. Several approaches have been used to improve these disadvantages of the ceramics.

One of the most popular approach to improve fracture toughness is the addition of ceramic reinforcements in the forms of particulates, whiskers, and fibers to form ceramic matrix composites (CMCs)[15-19]. Among these reinforcing forms, fibers has stronger reinforcing effect compare to particulates and whiskers. Continous carbon fibers have been widely used to reinforce ceramics[20-22]. The toughening mechanisms of fiber-reinforced CMCs are mainly attributed to the crack deflection at the fiber–matrix interface, crack bridging and fiber pull-out. It has been shown that weak fiber–matrix interfacial bonding resulting in the fiber pull-out toughening mechanism to operate.

Most recently, several new techniques have improved the properties of the ceramics/CNT nanocomposites, such as by tuning with dopants, new dispersions routes and modified sintering methods. Firstly, associated with the enhanced mechanical performance of Al_2O_3, the significantly improved wear resistance property of these composites could be suitable for some applications in automobile industry like valve seat, piston rings, and cylinder lines[23].

Yamamoto et al.[24] showed from scanning electron microscopy (SEM) observations on the fracture surface, the following features can be noted. First, there

are several individual MWCNTs protrude from the fracture surface, and the pullout of the MWCNTs can be clearly seen, which had not been obtained until now for conventional CNT-ceramic composites. Most of the CNTs are located in the intergranular phase with a length ranging from 0~10 μm. Second, in the case of the smaller amount of the acid-treated MWCNTs, no severe phase segregation was observed, whereas the composites made with the pristine MWCNTs revealed an inhomogeneous structure even for MWCNT addition as low as 0.9 vol.%. In addition to the above features, some MWCNTs on the fracture surface showed a ″clean break″ near the crack plane, and that the diameter of MWCNT drastically slenderized toward their tip, as illustrated in FIG. 2.3 (b) and 2.3 (c), respectively. As SEM cannot clearly resolve the thickness of a single MWCNT, TEM was used to determine if the fracture phenomenon of MWCNTs was indeed occurring during crack opening.

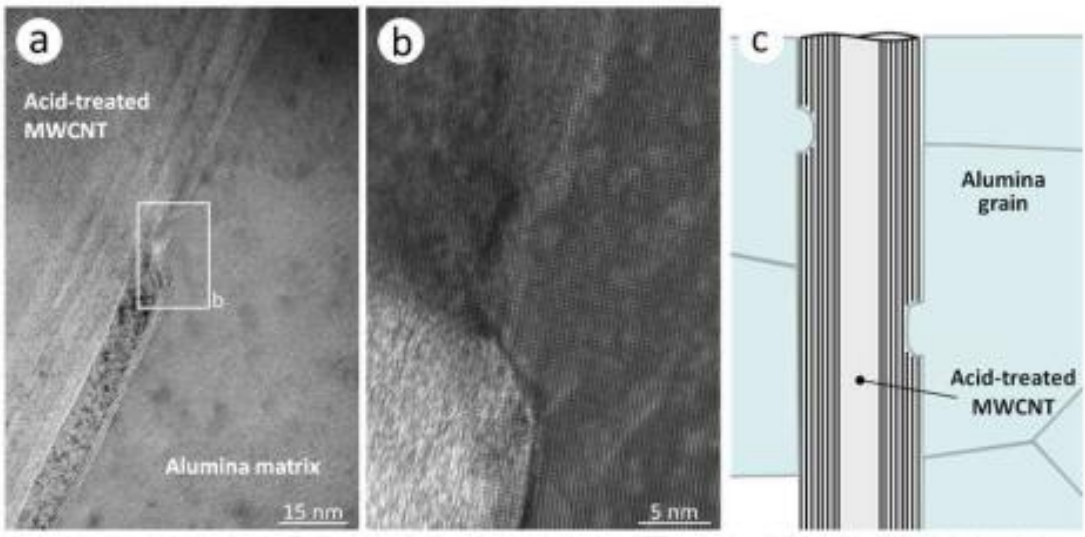

FIG. 2. 3 MWCNT morphology in the composites. (a) It is demonstrated that a nanodefect on the acidtreated MWCNT is filled up with alumina crystal. (b) Enlarged TEM image, taken from the square area. (c) Schematic description of MWCNT morphology in the composites (Figure 5 of Ref.24).

The pull-out of a carbon nanotube (CNT) from an alumina (α-Al_2O_3) matrix has been investigated by Liu et.al[25] using molecular mechanics simulations to study the interfacial properties due to van der Waals and electrostatic Coulombic interactions. They found out that the pull-out force of the CNT was found to be proportional to its diameter, but independent of its length and alumina grain boundary type. A theory was proposed to predict the force for an arbitrary pull-out of a CNT from the alumina matrix using the outermost wall diameter of CNT.

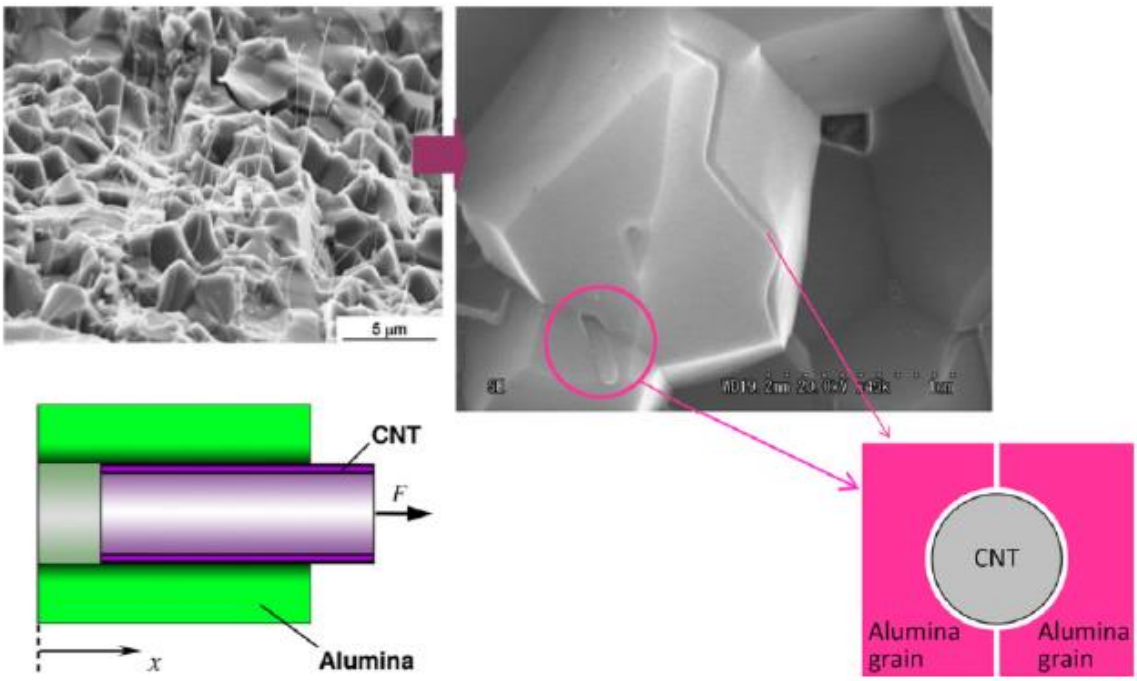

FIG. 2. 4 A SEM image of the fracture surface of CNT-alumina composites with CNTs located on GBs, and MM model for pull-out simulation (Figure 1 of Ref.25).

The toughening mechanisms of fiber-reinforced CMCs are mainly due to the crack deflection at the fiber–matrix interface and fiber pull-out mechanism. Usually, in general, strong interfacial bonding facilitates effective load transfer effect, but it prevents nanotube pull-out toughening from occurring. This is because strong interfacial bonding allows the crack to propagate straight through the fibers If the

interface cannot withstand the crack growth, resulting in low fracture toughness. The material strength to resist or deflect crack propagation in ceramics is very dependent on the ratio between covalent/ionic bonds.

2.4 Computational Details

A. Computational Methods

All the DFT calculations (Appendix A) in this study were performed using the plane-wave-based Vienna Ab-initio Simulation Package (VASP) [28-30]. The projector augmented-wave (PAW) [31-32] pseudopotentials were used to represent ionic cores, and the electronic kinetic energy cutoff for the plane-wave basis describing the valence electrons was set to 540 eV.

The **k**–point mesh of 4×4×1 Monkhorst-Pack mesh[33] was used in all calculations. The generalized gradient approximation (GGA) with the Perdew-Burke-Ernzerhof (PBE) functional [34-35] was selected in our calculations. The van der Waals (vdW) interaction plays an indispensable role in accurately determining the adsorption configuration and binding strength in this system. The effect of *vdW* interactions was taken into account by using the empirical correction scheme of Grimme (DFT + D/PBE),[36] which has been proved to be successful in describing the geometries of graphene-related structures (see Appendix B). Structural optimization was carried out on all systems until the residual forces were converged to 0.01 eV/A. The visualization of the crystal structures and the charge density differences were performed with VESTA[37]. The charge transfer between CNT and Ceramic surfaces can be more directly illustrated using Bader's Quantum Theory of Atom-in-Molecules approach [38], or in

short, the Bader charge. This Bader's charge analysis was performed considering charge contributions from both valence and core electrons.

Because the bonding between C atoms of CNTs and the atoms in ceramic surfaces is considerable, we examine these interactions by calculating the crystal orbital Hamilton populations and the respective integrated crystal orbital Hamilton populations (ICOHPs) using the linear muffin-tin orbital (LMTO) method[40]. The ICOHP counts the energy-weighted population of wavefunctions between two atomic orbitals for a pair of selected atoms up to the Fermi level; therefore, this value tends to scale with covalent bond strength (shared electron) contribution to interatomic bonding. The ICOHP analyses were performed using the LOBSTER package[40-42].

B. Computational Model

Although it provides a new view of the dependence of the composite mechanical properties on the CNT diameter, the resulting simulation results from Liu et.al have not yet matched the results of the experiments shown by Sun and Chena. Therefore this dissertation reports theoretical calculations by using Density Functional Theory to observe the effect of CNT diameter on the interaction between CNT and ceramics.

On DFT calculations, it is difficult to use the same model with the model used in mechanical molecular simulations. Beside the limitations of computational resources, involving so many atoms like the models used in molecular mechanical simulations, will take a lot of time.

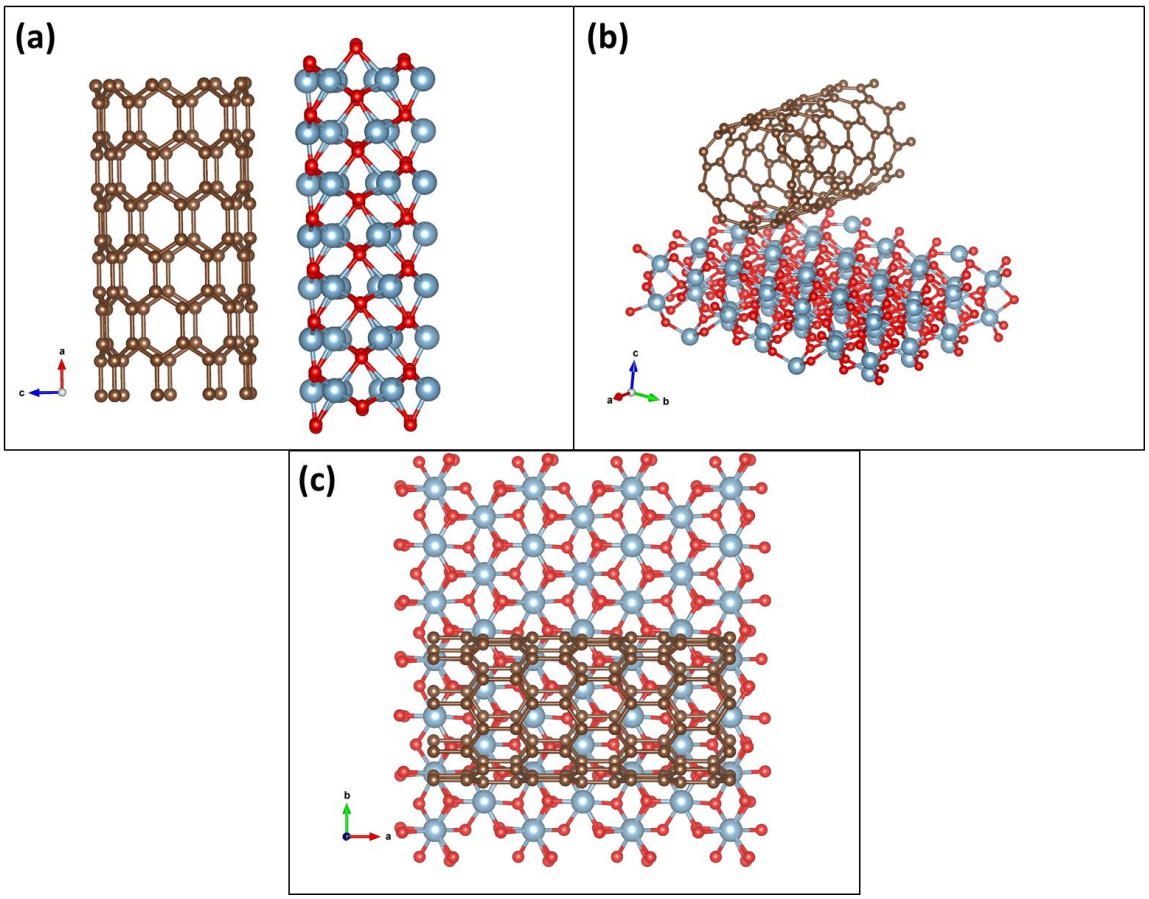

FIG. 2. 5 Computational Model (a) Side views (b) 3D view, (c) top view CNT on ceramic surfaces. The black lines represent the unit cell in calculations.

To investigate the interfacial interaction of ceramic and CNTs, we calculate CNTs on the flat ceramic surfaces in the tetragonal cell. In our models, the axial direction of the CNTs is set to be parallel to the surfaces (FIG. 2.5). The difference between tetragonal surfaces cell size and CNT length gives the interface lattice mismatch which leads to the strained of the CNT.

As interfacial configurations between CNTs and the ceramic surfaces, we calculate high symmetrical cases, where a surface atom is directly below either a CNT C atom, at the hollow site of CNT C atoms, or at the center of the C-C bridge site. Additionally, we also evaluate the other arrangement where the down most C atom of

CNT directly is above either the hollow site of surfaces atoms, or the center of the bridge site (see Appendix C).

References

1. S. Iijima, , Nature 354 (1991) 56–58.
2. J. Sandler, M. S. P.Shaffer, T. Prasse, W. Bauhofer, K. Schulte, A. H. Windle, Polymer, 40, 5967 (1999).
3. S. Curran, P. Ajayan, W. Blau, D. Carroll, J. Coleman, A. Dalton, A. P. Davey, B. McCarthy, A. Strevens,. Adv. Mater. 10, 1091 (1998).
4. P. A. Ajayan, L. S. Schadler, C. Giannaris, A. Rubio,. Adv. Mater. 12, 750 (2000).
5. M. S. P. Shaffer, A. H. Windle,. Adv. Mater. 11, 937 (1999).
6. Z. J. Jia, Z. Y. Wang, C. L. Xu, J. Liang, B. Q. Wei, D. H. Wu, S. W. Zhu,. Mater. Sci. Eng. A, 271, 395 (1999).
7. T. Kuzumaki, K. Miyazawa, H. Ichinose, K. J. Ito,. Mater. Res., 13, 2445 (1998).
8. A. Peigney, Ch. Laurent, A. Rousset, Key. Eng. Mater., 132-136, 743 (1997).. https://doi.org/10.4028/www.scientific.net/KEM.132-136.743
9. Ch. Laurent, A. Peigney, A. J. Rousset, Mater. Chem., 8, 1263 (1998).
10. Ch. Laurent, A. Peigney, O. Dumortier, A. J. Rousset, Eur. Ceram. Soc., 18, 1995 (1998).
11. A. Peigney, Ch. Laurent, E. Flahaut, A. Rousset, Ceram. Int., 26, 677 (2000).
12. S. Chang, R. H. Doremus, P. M. Ajayan, R. W. Siegel, Ceram. Eng. Sci. Proc., 21, 653, (2000). https://doi.org/10.1002/9780470294628.ch77
13. R. Z. Ma, J. Wu, B. Q. Wei, J. Liang, D. H. J. Wu, Mater. Sci., 33, 5243 (1998.)
14. Y. Sun and Q. Chena. Applied Physics Letters 95, 021901 (2009).
15. M. S. Dresselhaus, G. Dresselhaus, P. Avouris., Topics Appl. Phys. 80, 1–9 (2001).
16. M.S. Dresselhaus, G. Dresselhaus, J.C. Charlier, E. Hernandez. Phil. Transactions Roy. Soc. A. 362:2065-2098 (2004). DOI: 10.1098/rsta.2004.1430
17. E.T. Thostenson, Z.F. Ren, T.W. Chou. Comp. Sci. Tech. 61(13): 1899-1912 (2001)..
18. O. Breuer, U. Sundararaj. Poly. Comp.. 25(6): 630-645 (2004).
19. J.N. Coleman, U. Khan, W.J. Blau, Y.K. Gunko. Carbon. 44:1624- 1652 (2006).

20. M. Moniruzzaman, K.I. Winey, Macromolecules. 39(16): 5194-5205 (2006).
21. A. Peigney, C. Laurent, E. Flahaut, et al. Ceram. Intl. 26(6): 677-683 (2000).
22. W.A. Curtin, B.W. Sheldon, Materials Today. 7(11):44-49 (2004).
23. G.D. Zhan, J.D. Kuntz, J. Wan, Ak. Mukherjee. Nat. Mat.. 2:38-42 . (2003).
24. G. Yamamoto, T. Hashida, *Open access peer-reviewed chapter* "Composites and Their Properties". Ch.21. DOI: 10.5772/48667, (2011).
25. S. Liu et al, CARBON, 49, 3701-3704,(2011)
26. G. Kresse and J. Hafner. Phys. Rev. B, 47, 558 (1993).
27. G. Kresse and J. Hafner. Phys. Rev. B, 49,14251 (1994).
28. G. Kresse and J. Furthmüller. Comput. Mat. Sci., 6, 15 (1996).
29. G. Kresse and J. Furthmüller. Phys. Rev. B, 54, 11169 (1996).
30. G. Kresse, D. Joubert, Phys. Rev. B 59, 1758 (1999).
31. P.E. Blochl, Phys. Rev. B 50, 17953 (1994).
32. H. J. Monkhorst, J. D. Pack, Phys. Rev. B 13, 5188 (1976).
33. J. P. Perdew, K. Burke, and M. Ernzerhof, Phys. Rev. Lett., 77, 3865 (1996).
34. S. Entani, L.Y. Antipina, P.V. Avramov, et al. Nano Res. 8: 1535 (2015). https://doi.org/10.1007/s12274-014-0640-7
35. J. P. Perdew, K. Burke, and M. Ernzerhof, Phys. Rev. Lett., 78, 1396 (1997).
36. S.J. Grimme, Comput. Chem. 27, 1787 (2006).
37. K. Momma, F. J. Izumi, Appl. Crystallogr. 44, (2011), 1272−1276.
38. G. Henkelman, A. Arnaldsson, H. Jonsson, Comput. Mater. Sci. 36, 354−360. (2006).
39. R. Dronskowski, and P. E. Blochl. *J. Phys. Chem.* **97**, 8617–8624 (1993)
40. V. L. Deringer, A. L. Tchougreeff, and R. J. Dronskowski. Phys. Chem. A, , 115(21), (2011) 5461-5466.
41. S. Maintz, et al. J. Comput. Chem., 34(29), (2013) 2557-2567.

Chapter 3 Zigzag CNTs and Graphene Structure

3.1 Introduction

The great interest in one-dimensional nanostructures such as nanotubes and nanowires is partly driven by the possibility of their being used as active components in nanosized devices. Carbon nanotubes (CNTs), discovered in 1991 by Ijima, are considered to be a very important and interesting class of nanostructures due to their unique electrical, mechanical and thermal properties, and possibility of their industrial applications. A single wall carbon nanotube (SWCNT) is formed by rolling a two-dimensional grapheme sheet, which has a planar crystalline structure made with hexagonal carbon rings. A multiwall nanotube is made up of more than one SWCNTs of different diameters which share a common axis. Understanding the properties of individual SWCNTs and the interaction between them is important to understand the properties of multiwall CNTs as well as SWNTs in a bundled form. Diameter of SWCNTs is typically of the order of a few nanometers and their length typically exceed a micrometer. Cabria et al[1] has shown through first principles calculations of the electronic structures of narrow zigzag CNTs revealed that tubes with diameter < 0.4 nm

are unstable. However, effect of curvature (diameter) on the physical properties of zigzag CNTs deserves to be understood in detail.

3.2 Results and Discussions

As the first step in our study, we studied the curvature effect of the single-walled CNTs with different diameters and graphene as a CNT with an extremely large diameter. We calculated the metallic zigzag types of CNTs with (3,0), (6,0), (9,0) and (12,0) and graphene to investigate the CNT-diameter dependence of the interaction between CNT and ceramic surfaces. Results of the structural and geometrical properties of different zigzag CNTs report that lattice constant in the axial direction of the CNTs ranges from 4.22 – 4.27 Å depicted in the Table 3.1.

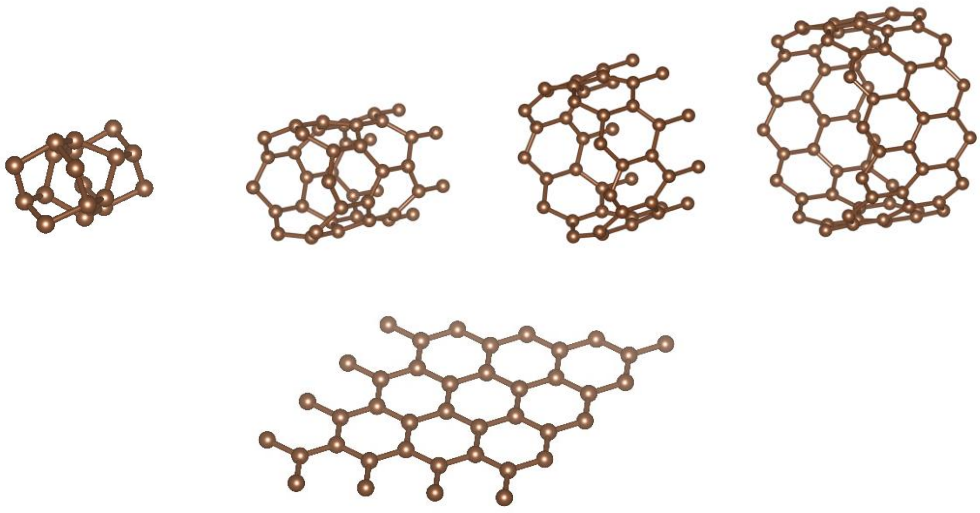

FIG. 3. 1The diameter and length of CNTs of (3,0), (6,0), (9,0), (12,0)[5] and graphene (from left to right respectively) used in this work.

TABLE 3. 1 Comparison of the values of lattice constant along the axis of CNT of c (Å), bond length of l_b (Å),cohesive energy per atom of E_c (eV/atom) and bandgap of E_g (eV) for zigzag CNTs with different chirality index of n.

System (n,0)	c (Å)	l_b (Å)	d (Å)	E_c(eV/atom)	E_g(eV)
(3,0)	4.22	1.410	2.67	8.027	0.00
(6,0)	4.26	1.411	4.75	8.851	0.00
(9,0)	4.27	1.420	7.03	9.037	0.00
(12,0)	4.27	1.422	9.34	9.107	0.00
Graphene	-	1.425	-	9.199	0.00

The C-C bonds in the CNTs are found to deviate from their ideal values of 1.425 Å in the unrolled graphene sheet but in general, this result is in a good agreement with the result from Kahaly[2] and Cooper et al[3].

We then calculate cohesive energy because is an important physical quantity that accounts for the bond strength of a solid, which equals the energy needed to divide the solid into isolated atoms by breaking all the bonds.

$$E_{coh} = \frac{E_{tot} - \sum NE_{iso}}{N}$$

With E_{tot} as the total energy of the bulk, E_{iso} as the total energy of an isolated atom, and N as the number of atoms in the units cell.

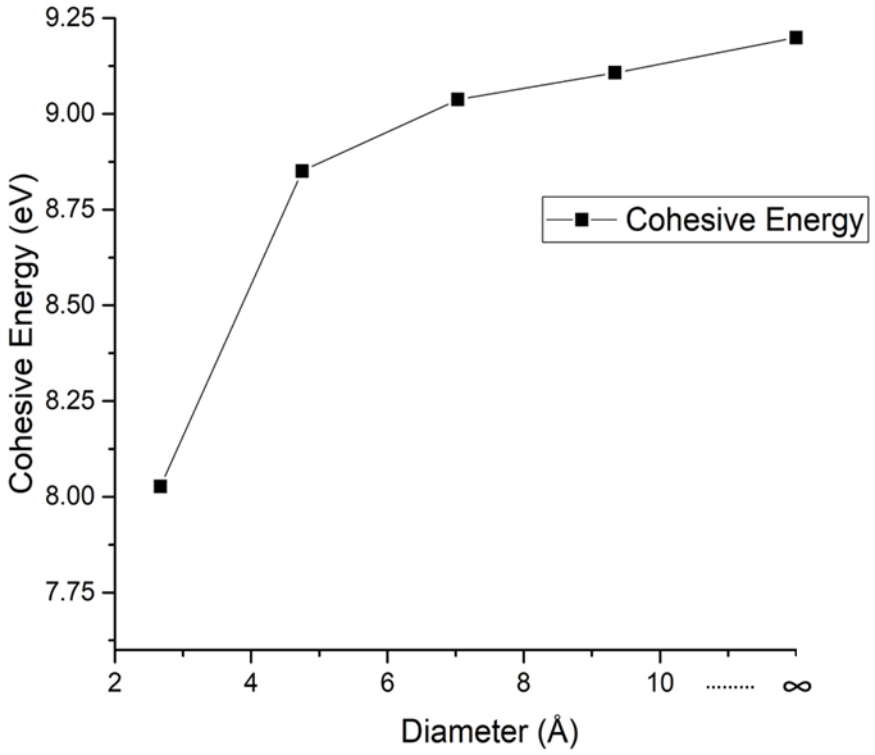

FIG. 3. 2 Cohesive energy of CNT as a function of diameter

Cohesive energy of all CNTs increases with chirality index, *n* (increasing diameter) as shown in FIG. 3.2. However, this difference diminishes as the diameter of the tube increases or the curvature reduces.

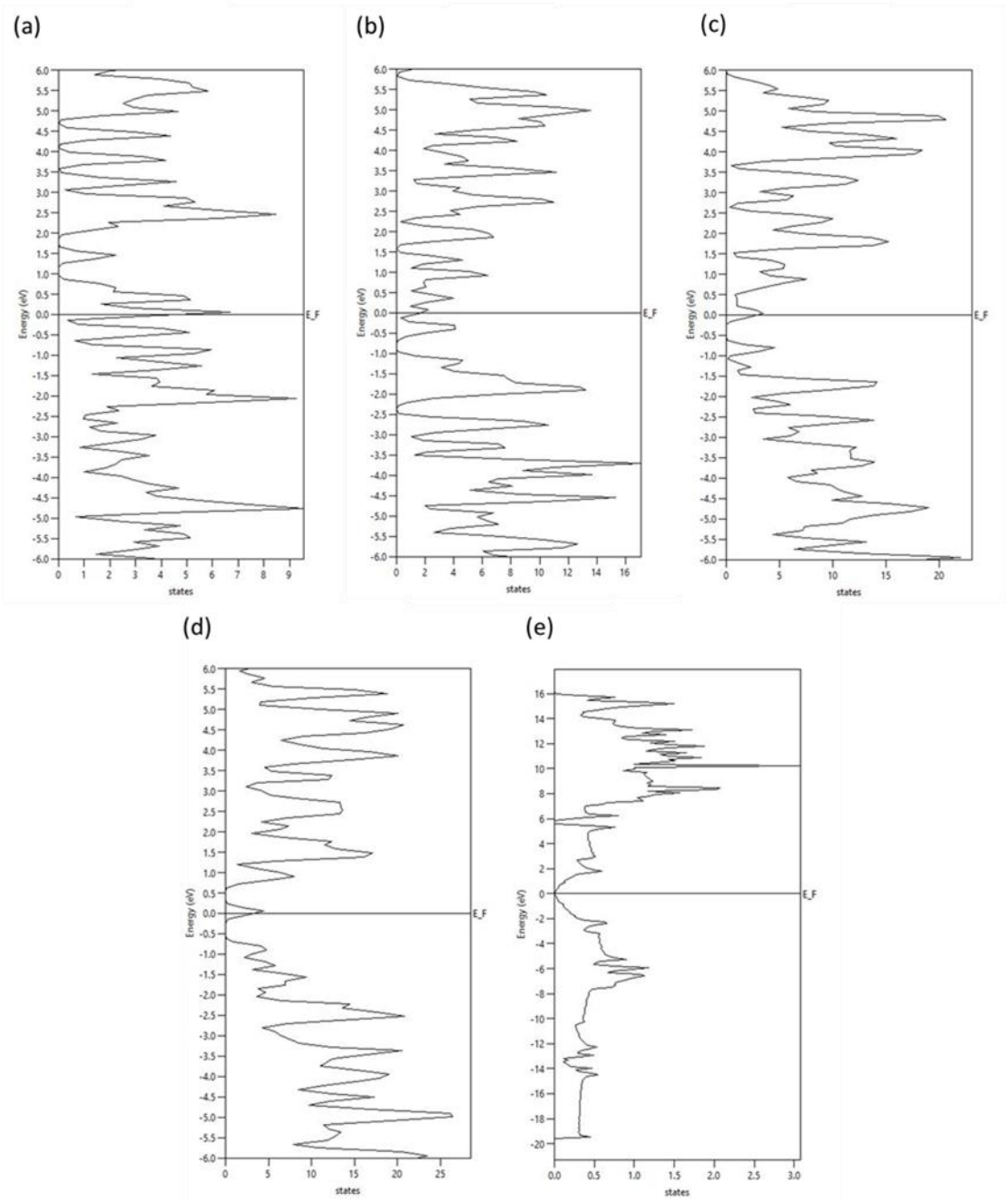

FIG. 3. 3 Electronic densities of states (DOS) of (a) (3,0), (b) (6,0), (c) (9,0), (d) (12,0), CNTs and (e) graphene.

As shown in FIG. 3.3(a)-(e), the comparison between the DOS of the (3,0), (6,0), (9,0), (12,0) CNT and graphene respectively indicates that all the CNTs are metallic with zero bandgap. This result in agreement with the experimental results by Odom et al[4], the DOS of each of these nanotubes (with diameter < 10 Å) is asymmetric outside

the energy interval of ± 1 eV about the Fermi level. This reflects on the interactions among electronic states with energies close to the Fermi energy. As the diameter of the nanotube increases, the DOS of a nanotube becomes increasingly symmetric about the Fermi level.

3.3 Conclusion

We used first-principles DFT calculations to understand structural properties of zigzag carbon nanotubes. Cohesive energy of CNT increases with increasing diameter. Curvature effects are most prominent for CNTs with smaller diameter and well understood.

References

1. I. Cabria, J. W. Mintmire and C. T. White. Int. J. Quant. Chem., 91, 51, (2003).
2. M.U. Kahaly, U.V Waghmare, Bull. Mater. Sci., Vol. 31, No. 3, (2008).
3. D.Cooper, B. D'Anjou, N. Ghattamaneni, et al. ISRN Cond. Matt. Phys., vol. 2012, Article ID 501686, (2012). doi:10.5402/2012/501686
4. T. W. Odom, J. L. Huang, P. Kim and C. M. Lieber. J. Phys. Chem. B104 2794. (2000).
5. I. D Aditya ,. D. Matsunaka, Y. Shibutani, G. Yamamoto, J. Appl. Phys. 121, 025304 (2017)

Chapter 4 Interfacial Interaction between CNT and Al_2O_3

4.1. Introduction

Experimental investigations showed that Al_2O_3 composites with CNTs[1-4] have enhanced mechanical properties of 689.6 ± 29.1 MPa for bending strength and 5.90 ± 0.27 $MPa \cdot m^{1/2}$ for fracture toughness. In order to develop ceramic composites reinforced with carbon materials, it is important to understand the interfacial properties of ceramic and carbon materials. Most recently, several new techniques have improved the properties of the ceramics/CNT nanocomposites, such as by tuning with dopants, new dispersions routes and modified sintering methods. Firstly, associated with the enhanced mechanical performance of Al_2O_3, the significantly improved wear resistance property of these composites could be suitable for some applications in automobile industry like valve seat, piston rings, and cylinder lines[5]. Additionally, outstanding electrical properties of CNTs make ceramic materials such as Al_2O_3 attractive for specific applications like electromagnetic/antistatic shielding of electronic components, electrical igniters, electrodes for fuel cells, crucibles for vacuum induction furnaces and electrical feed through[6-11]. Electric conductivity (EC) of ceramics reinforced with

single-walled (SW) CNTs (106 S/m) increases more than with multi-walled (MW) CNTs (103 –105 S/m) [12-13].

First-principles studies on interfacial interactions of CNTs with various materials have been investigated. Orellanna et al.[14] have found that the properties of CNT adsorbed on Si(001) are changed. Zhao et al.[15] suggested that Ni surfaces can catalytically weaken the C–C bonds near the Ni–C interface. David et al.[16] proposed that the C-C σ bonds of CNTs are broken when they are adsorbed on Ni surfaces. Furthermore, the Ni–C bonds become stronger as a carbon nano arch is formed on the Ni surfaces. These results showed that debonding of the C-C σ bonds of CNT is catalytically induced on Ni surfaces. Meanwhile, an interfacial interaction between CNT and ceramic surface, especially Al_2O_3, has not been explored, by first-principles calculations.

On the other hand, interfacial interactions of various adsorbance on Al_2O_3 surfaces also have been explored. Li et al. [17] in which they analyzed the adhesion nature for a series of metals including Al, Ni, Cu, Au, Ag, Rh, Ir, Pd, Pt, Nb, and β-NiAl on Al_2O_3 surfaces. They reported that chemical bonding is found to be metallic for the Al-rich interfacial stoichiometry, primarily ionic with some covalent contributions for the O-rich stoichiometry. Another study on single-layer graphene on $Al_2O_3(0001)$[19] has reported that the electronic properties of the graphene on the O-terminated Al_2O_3 surface are completely different from that on the Al-terminated one. It was shown that graphene has a strong interaction with O-terminated Al_2O_3 surface, which is caused dominantly by the electrostatic force involved in the graphene π-system and the unsaturated electrons of the topmost O layer rather than the van der Waals interactions[19].

Yamamoto et al. showed (Fig.4.1) from transmission electron microscopy (TEM) observations and single nanotube pullout experiments on the CNT- Al_2O_3 composites. They reported that while some CNTs were pulled out from the Al_2O_3 matrix in fracture[8], the sword-in-sheath mode[9,10] was also observed, in which the outer wall of multi-walled CNTs was broken and the inner part was pulled out. It means that the outer walls of the CNT have a very strong bonding with the Al_2O_3 matrix.

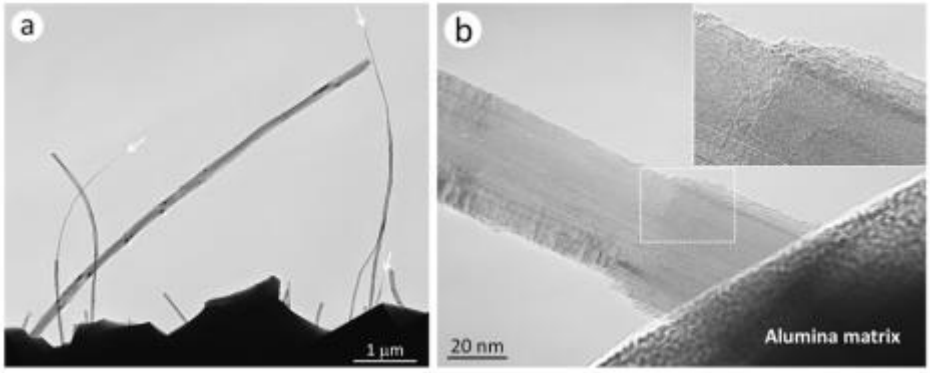

FIG. 4. 1 TEM images of the fracture surface of the composite acquired (a) low and (b) high magnification images.[4]

This pullout behavior resulting in an increase in fracture toughness as shown in the following table:

TABLE 4. 1 Mechanical properties of CNT-Al_2O_3 composite by Yamamoto[4]

Materials	Relative density (%)	Bending strength (GPa)	Fracture Toughness (MPa $m^{1/2}$)
Al_2O_3	100	502.3	4.33
Al_2O_3 + 0.9 vol % MWNT	100	689.6	5.90
Al_2O_3 + 1.9 vol % MWNT	100	646.8	5.63

The addition of CNTs increases the fracture toughness of alumina to more than 100%. Crack deflection along the continuous interface between carbon nanotubes and nanocrystalline alumina matrix grains observed by Zhan is possibly one of the toughening mechanisms[24]. He also observed that CNT were strongly entangled with the alumina matrix. To understand the pullout behavior of the CNTs, Liu et al.[17] have performed molecular dynamics studies of interfacial sliding and friction in CNT-reinforced diamond composites (Fig.4.2) and obtained the interfacial strength in the range of 1–40 MPa. Li et al.[18] have conducted a similar study with an amorphous carbon matrix and suggested the interfacial strength in the range of 20–120 MPa. They proposed that the pull-out force is only proportional to the nanotube diameter and independent of the nanotube length and the GB structure of the Al_2O_3 matrix.

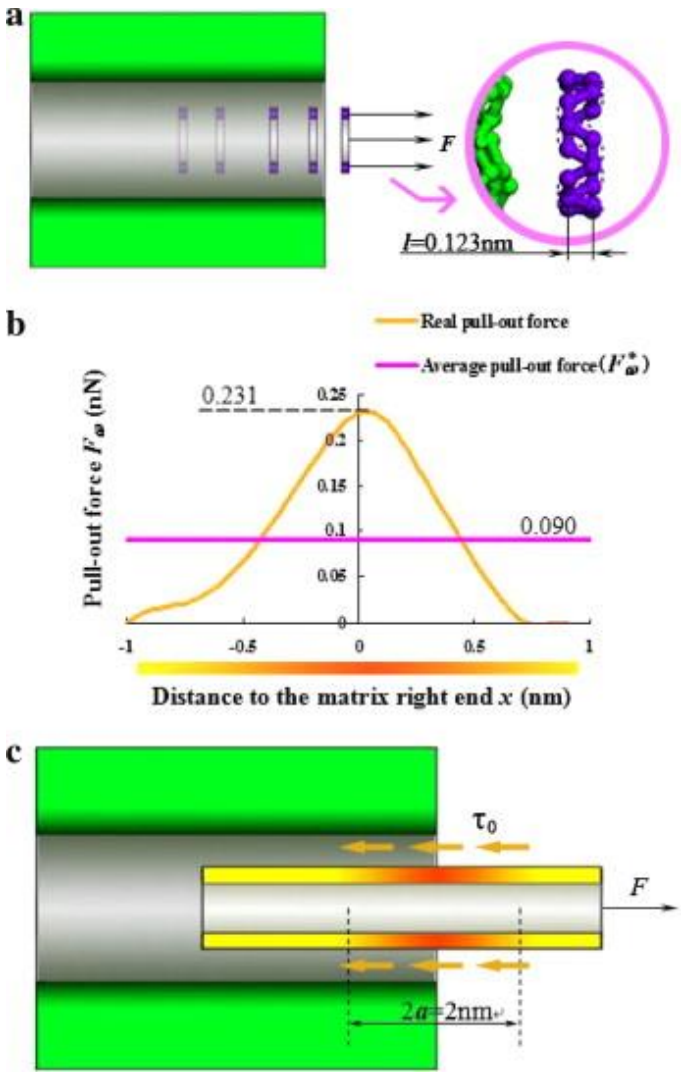

FIG. 4. 2 Molecular Dynamics simulation of interfacial sliding and friction in CNT-reinforced alumina composites by Liu et al.[25]

The CNT's surface unevenness and its anchoring with the ceramics matrix are a good physical explanation of enhanced frictional forces at the interface. However, the interfacial bonding of CNTs with the ceramics remained unexplained for several years. The understanding of the nanostructure characteristics and the interfacial relationship between CNTs and the ceramic matrices is far from satisfactory, which opens new windows of potential research in this advanced area of nanotechnology [3-4,12].

4.2 Results and Discussions

A. Al_2O_3 Bulk and Surface

The bulk structure of Al_2O_3 has hexagonal symmetry ($R\bar{3}c$) [20]. The calculated lattice parameters of bulk structure of Al_2O_3 were a =4.783 Å and c = 13.012 Å, which are in good agreement with experimental values of a = 4.758 Å and c = 12.991 Å[21-23], a = 4.76 Å and c = 12.993[25].

Previous theoretical calculations demonstrated that an Al-terminated surface was the most stable one[26-27]. As various types of interface structures could be generated in Al_2O_3 composites with CNTs through the processing, the O-terminated systems are also investigated in this study. The Al-terminated (O-terminated) Al_2O_3(0001) is modeled by a slab containing seven O layers and six (five) Al layers with a 20 Å vacuum region in a tetragonal cell (FIG.4.4). The atomic structure of the O-terminated systems is constructed by removal of the top surface Al atoms from the Al-terminated systems. For the Al-terminated and O-terminated surfaces, the amounts of changes of the interlayer spacings are listed in TABLE 4.2.

TABLE 4. 2 Relaxation of interlayer spacings of Al-terminated and O-terminated Al_2O_3(0001) in terms of percent of the bulk geometry spacings. Δd_{mn} represents the amount of change of the interlayer spacing between m -th and n -th adjacent surface layers.[37]

	Al Terminated					O Terminated			
	This work	Ref [27]	Ref [28]	Ref [29]	Ref [30]	This work	Ref [31]	Ref [32]	Ref [33]
Δd_{12}(%)	−82.3	−84.5	−85.5	−87.4	−82	−7.6	−13.2	−7.2	−14.4
Δd_{23}(%)	+6.25	+3.5	+3.2	+3.1	+7	−8.6	−6.9	−1.5	−10.3
Δd_{34}(%)	−43	−45.8	−45.4	−41.7	−52	+11.4	+13.5	+7.3	+15.3
Δd_{45}(%)	+ 18.5	+19.4	+19.8	+18.9	+25	−1.9	−7.7	−0.6	−5.9

For the Al-terminated surface, the top surface Al atoms underwent large relaxations of 82.3% and the second surface O layer moved little inward by 6.25%. Consequently, these surface Al and O layers were almost coplanar with the second surface O layer. For the subsurface layers as well as the top surface layer, the relaxation is significant. It implies that the necessity of using a relatively thick slab for a good description of the Al-terminated α-Al_2O_3 (0001). The inward relaxation of the top layer of the O-terminated surface is smaller than for the Al-terminated surface. As shown in TABLE 4.1, the results are in agreement with the other DFT studies[28-34], although they differ slightly due to the exchange-correlation functional[34].

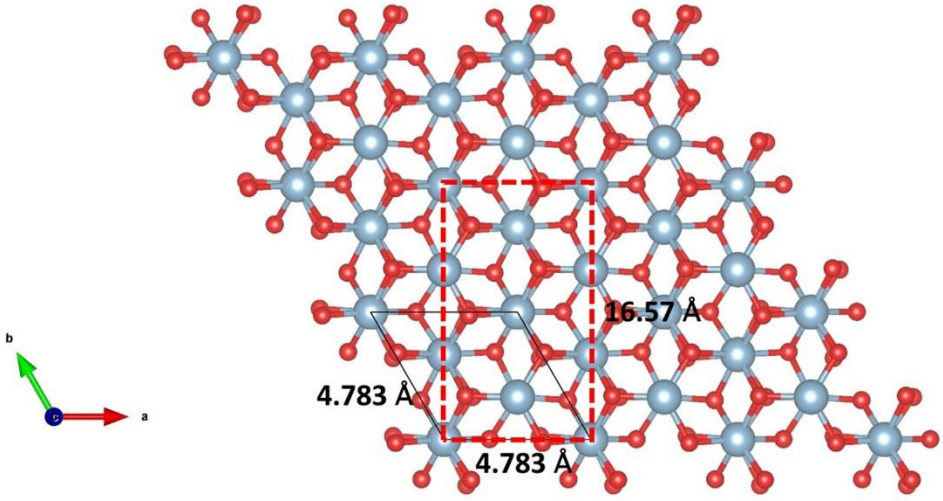

FIG. 4. 3 Al_2O_3 (0001); Black straight line and red dashed line correspond to rhombohedral and tetragonal unit cell respectively.[37]

To investigate the interfacial interaction of Al_2O_3 and CNTs, we calculated CNTs on the Al_2O_3 (0001) in the tetragonal cell. In our models, the axial direction of the CNTs is set to be parallel to $[10\bar{1}0]$ on the Al_2O_3(0001) (FIG.4.4). The difference between tetragonal Al_2O_3(0001) cell size and CNT length gives the interface lattice mismatch of

about 0.5 Å (~11 %) which leads to the strained of the CNT. Because of the large mismatch, the band structure of the strained CNTs in our models is marginally changed and then they are not all completely metallic. Although this requires a careful consideration for quantitatively accurate evaluation of the interface interaction obtained in this study, it is possible to discuss effects of the CNT diameter on the interfacial interaction between CNT and Al_2O_3.

As interfacial configurations between CNTs and the Al_2O_3(0001)s, we calculated high symmetrical cases, where a surface Al or O atom is directly below either a CNT C atom, at the hollow site of CNT C atoms, or at the center of the C-C bridge site. Additionally, we also evaluate another arrangement where the down most C atom of CNT directly is above either the hollow site of Al-O surface atoms, top of Al or O atom, or the center of Al-O bridge site (see Appendix B).

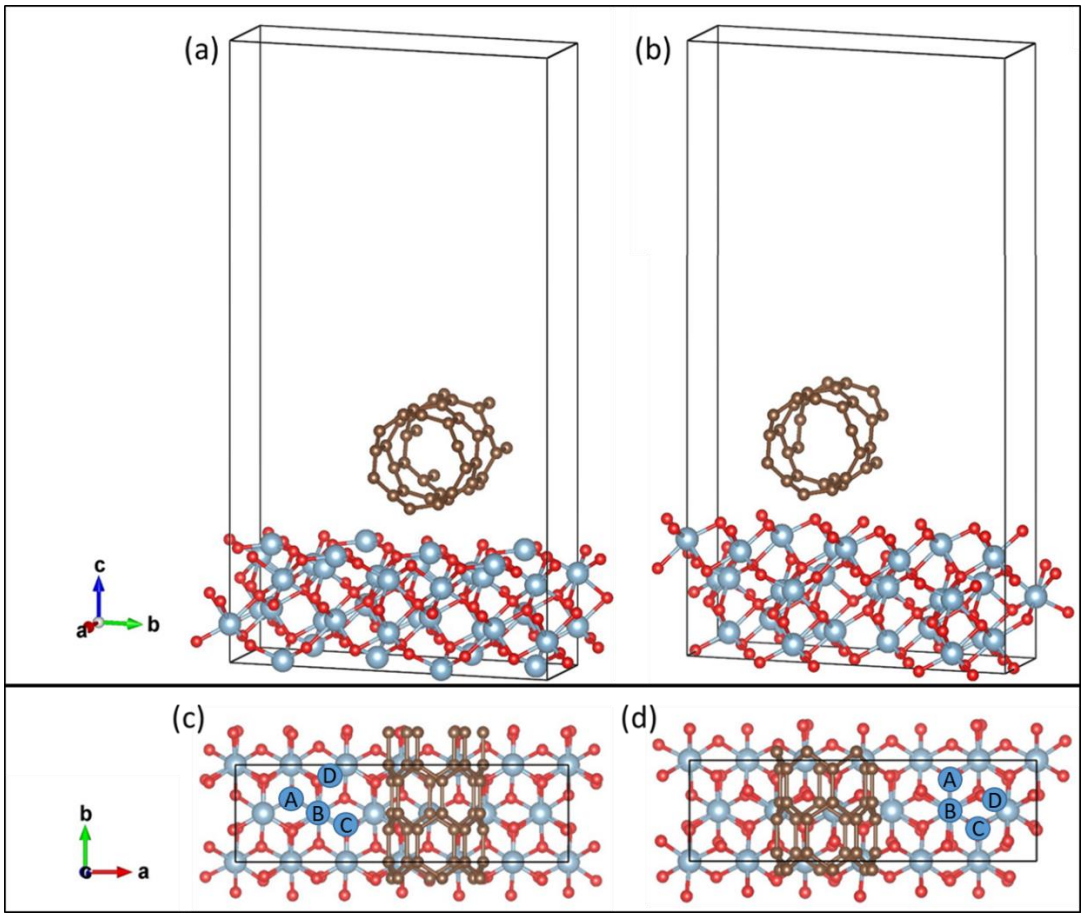

FIG. 4. 4 Side views of CNT on (a) Al-terminated, (b) O-terminated, and top views (c) Al-terminated, (b) O-terminated Al_2O_3(0001). The brown, red, and gray balls denote the C, O, and Al atoms, respectively. The black lines represent the unit cell in calculations.[37]

B. Adhesion behavior of CNT/ Al_2O_3 (0001) interfaces

To reveal the nature of the interfacial bonding between CNT and Al_2O_3 (0001), FIG. 4.5 depict the 2D and 3D charge density difference, for the interfaces of the CNTs and each of the Al–terminated and O-terminated Al_2O_3(0001), respectively. The difference of the charge density, $\Delta\rho(r)$, is calculated to investigate the CNT–surface interfacial bonding using Eq.(4.1).:

$$\Delta\rho(r) = \rho_{CNT-S}(r) - \rho_{CNT}(r) - \rho_S(r) \tag{4.1}$$

It has been done by subtracting the combined charge of the isolated surface (without CNT) of $\rho_S(r)$ and CNT (without surface) of $\rho_{CNT}(r)$ from the charge of the CNT-surface interface system of $\rho_{CNT-S}(r)$ by setting the atom configurations of the isolated surface and CNT as the CNT-surface interface system.

The structures of the CNT and Al-terminated Al_2O_3(0001) hardly change from those before adsorbing as shown in FIG. 4.5. The interfacial C-Al interatomic distance is about 2.11 Å for (3,0) CNT, 2.37 Å for (6,0) CNT, 2.82 Å for (9,0) CNT, and single C-Al bond with the length 2.77 Å for (12,0) CNT, respectively. The C-Al bond length for small CNTs of (3,0) and (6,0) is shorter than large diameter CNTs of (9,0) and (12,0).

The interfacial bonding interaction with the Al-terminated Al_2O_3 (0001) is almost similar for all CNTs. The localized charge accumulation is observed between the down

most C atom of CNT and the topmost Al atom of Al_2O_3(0001). This implies that the down most C atom of CNT is interacted with the topmost Al atom of Al_2O_3(0001) by forming covalent bonding.

When CNTs come close to the O-terminated surface, their shape was changed, unlike on the Al-terminated surface. The degree of the shape change depends on the diameter. For the smallest diameter CNTs, the tube shape of CNT was broken and it transformed into an arch-like structure, as the previous first-principles calculation of CNTs on Ni performed by David et al[16]. The edge C atoms of the arch-like structure have interfacial bonds. As shown in Fig 4.5(f)-(i), the localized charge accumulation is apparent between the edge C and the surface O atoms. This adsorbing process involving spontaneous dissociation of C-C σ-bonds shows that the O-terminated Al_2O_3 (0001) has a catalytic effect and the activation energy barrier for the bond breaking would be vanishingly small. On the other hand, for the larger diameter CNTs of (6,0), (9,0), and (12,0), the change in the structures diminishes and the catalytic effect is relatively weaker.

The C-O interatomic distances of the interfaces depend on the diameters of CNTs; 1.26 Å to 1.42 Å for (3,0) CNT, 1.27 Å to 1.29 Å for (6,0) CNT, 1.38 Å to 1.40 Å for (9,0) CNT, and 1.37 Å to 1.41 Å for (12,0) CNT. The C-O interatomic distance for smaller CNTs is shorter than larger diameter CNTs, implying that the adhesion interaction of the CNTs on Al_2O_3 (0001) is weakened as increasing the CNT diameter. This result shows that the strong interfacial interaction of smaller CNTs with the O-terminated Al_2O_3 (0001) would be a possible mechanism for the successful Al_2O_3 composite reinforced with CNTs.

We think that the interfacial bonding of CNT and O-terminated Al_2O_3 (0001) is of mixed covalent-ionic nature. This interfacial bonding has the same characteristic as the interface of metal and O-terminated Al_2O_3 obtained by Li et al[17]. The strong ionic-covalent interfacial bond is the primary reason why the adhesive energy between CNTs and the O-terminated Al_2O_3(0001) is always the largest in comparison with those of the Al-terminated surface.

The interfacial bonding of the O-terminated interface is formed by strong hybridization and charge transfer between C atoms of the CNTs and O atoms of the Al_2O_3, namely strong covalent and ionic interactions. This result is related to the interfacial stoichiometry. The Al-terminated Al_2O_3 (0001) is reduced to a stoichiometric surface due to relaxation of the top surface Al atoms. On the other hand, for the O-terminated surface, the inward relaxation of the top surface layer is smaller, and a non-stoichiometric atomic configuration remains. Hence some charge transfer would occur easily from the C atoms of the CNTs to the top surface O atoms in order to compensate electrons. Prior study of interfacial interaction between CNT and other oxides surface also supports this idea by saying that O-terminated surface provides stronger interaction due to the electron affinity between C and O[34].

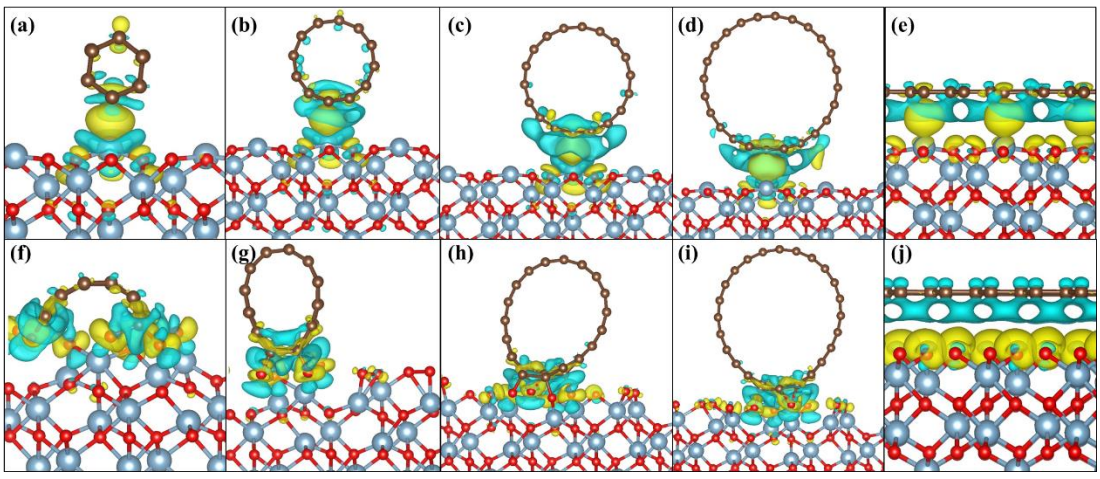

FIG. 4. 5 Calculated charge density difference for the most stable configuration between: (a) (3,0), (b) (6,0), (c) (9,0), (d) (12,0) CNTs, (e) graphene and Al-terminated Al_2O_3(0001) and (f) (3,0), (g) (6,0), (h) (9,0), (i) (12,0) CNTs, (e) graphene and O-terminated Al_2O_3(0001) respectively. Color key: brown, grey, and red denote the C, Al, and O atoms, respectively with Isosurface level for (a)-(b) : 0.00032 $e^-/Å^3$; (c)-(e) : 0.00081 $e^-/Å^3$; while (f)-(i) : 0.0066 $e^-/Å^3$ and (j) : 0.0017 $e^-/Å^3$ [37].

C. Interface structures and bonding of CNT/ Al_2O_3 (0001)

Our DFT calculations showed significant differences in the interfacial bonding characteristics for the two types of Al_2O_3 (0001) according to the surface termination. In the case of the O-terminated Al_2O_3 (0001), especially for small diameter CNTs depicted in FIG. 4.5 (f) and (g), the tube structure of CNTs did not hold. To quantitatively evaluate the interfacial interaction of CNTs and Al_2O_3, the adhesion energy, defined as the energy needed to separate the surfaces that conform the interface, is calculated as

$$E_{adh} = \frac{E_{CNT-S} - \left(E_{CNT} + E_S\right)}{A(D)} \tag{4.2}$$

Where E_{CNT-S} is energy of the CNT/ceramic surface system, E_{CNT} is energy of the isolated single CNT, E_S is energy of the ceramic surface, and $A(D)$ is the projected contact area of CNT on the ceramic interface dependent to CNT diameter *D*. The calculated adhesion energy results are showed as a function of the CNT diameter, in FIG. 4.5.

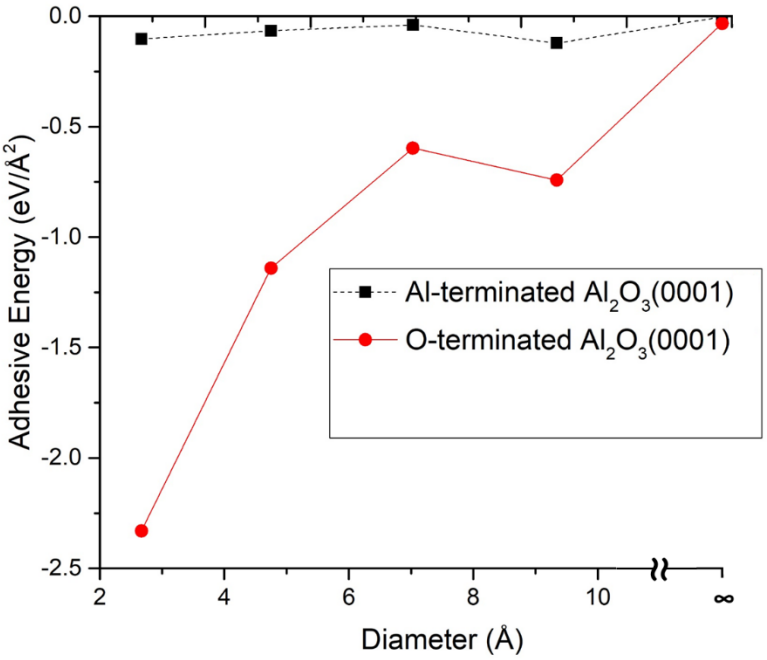

FIG. 4. 6 Adhesive energy as a function of CNTs diameter[37]

The adhesion energy of CNTs on the O-terminated surface is much stronger than on the Al-terminated surface. The qualitative trend of the adhesion energy correlates to the interfacial interatomic distances and the charge density difference of the CNT-Al_2O_3(0001) interfaces. For the O-terminated interface, the adhesion energy of the CNT of (3,0) is much lower compared with the other CNTs, because of the strong bonding of the dissociated C atoms of the CNT with the surface O atoms. The Al_2O_3-induced dissociation of CNTs which leads to the strong interfacial bonding would be a possible mechanism for a successful Al_2O_3 composite reinforced with CNTs. Crack deflection along the continuous interface between carbon nanotubes and nanocrystalline alumina matrix grains observed by Zhan[24] is possibly one of the toughening mechanisms. He also observed that CNT were strongly entangled with the

alumina matrix; The results we obtain support this argument as shown by the adhesive energy between CNT and O-terminated Al_2O_3 (0001) which is very strong.

According to Li. Et al[17], O-terminated (O rich) interface of Al_2O_3(0001) has very strong ionic-covalent bonding. To know the contribution of these covalent and ionic bonds and their relation to the diameter of the CNT, we use the ICOHP and Bader charge transfer (see Appendix B).

The ICOHP values also shows that smaller CNT has stronger covalent bonding with higher ICOHP values. Moreover, it can be seen that the values of ICOHP are roughly inversely proportional to CNT diameter, i.e., the larger ICOHP values correspond to smaller diameter CNT and possible stronger covalent interactions[31-34]. Covalent interaction for O terminated is stronger compared to Al terminated surface. Results of a Bader charge transfer support and elucidate our result on adhesive energy for each interaction between CNTs and ceramic surfaces from which the bonding interaction comes from. The strongest adhesive energy of CNTs and O-terminated Al_2O_3 comes from both strong covalent and ionic bonding between C atoms of the CNT and oxygen surface. These strong covalent and ionic interaction shown between CNTs with Al_2O_3 are likely to cause crack deflection propagates in the interface very slowly and this may further assist in the prevention of crack initiation, possibly increasing the composite's toughness as a result obtained by Zhan[24].

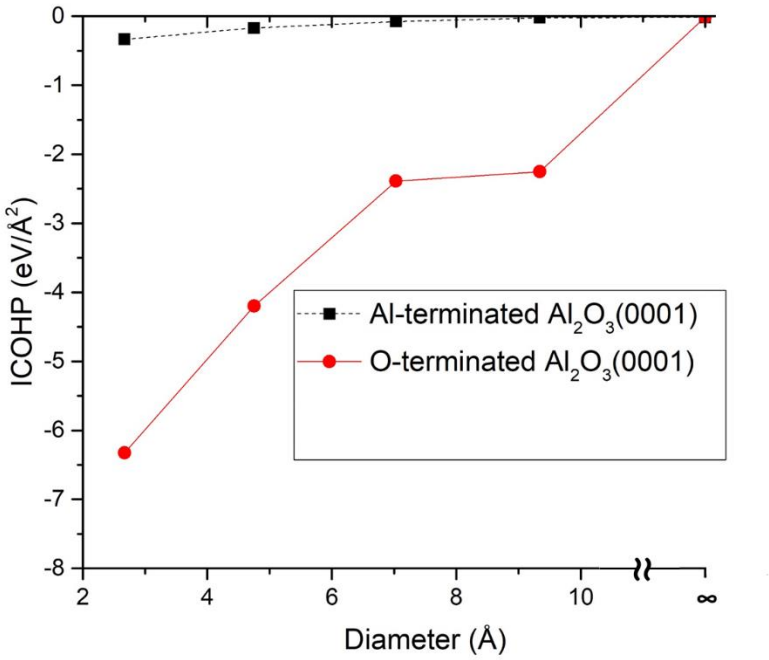

FIG. 4. 7 ICOHP as a function of CNTs diameter

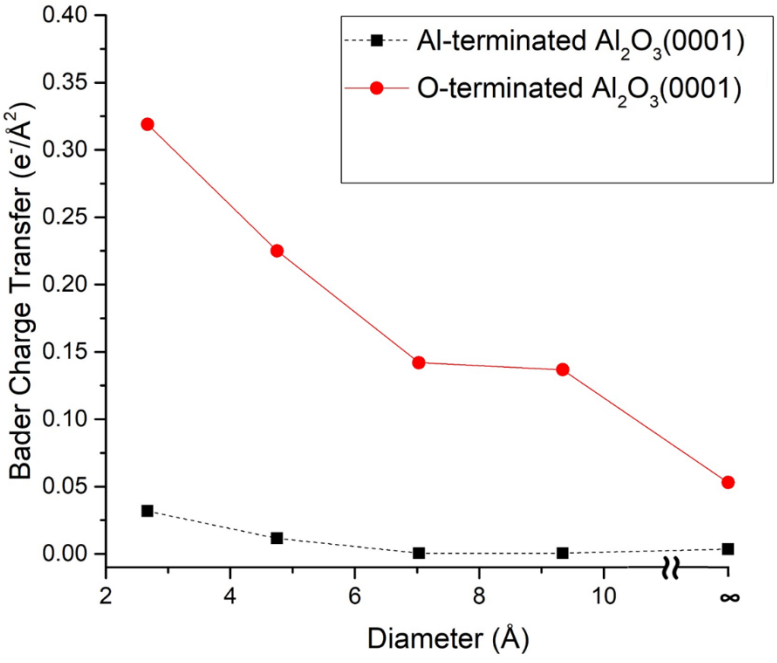

FIG. 4. 8 Charge transfer as a function of CNTs diameter

4.3 Conclusion

In this study, we investigated the interaction of CNTs and Al_2O_3(0001) using first-principles calculations. On Al-terminated surface, the structures of all the CNTs do not drastically change from those before adsorbing. Meanwhile, for the O-terminated surface, the structure of all CNTs is changed depending on the diameter.

The interfacial interaction between CNTs and the O-terminated surface has the mixed covalent-ionic nature. Especially, the small diameter CNT has a strong interaction with the O-terminated surface, which is caused by the opening of CNTs and the successive transform into an arch-like structure. This behavior means that the O-terminated Al_2O_3(0001) has a catalytic effect and the activation energy for dissociation of C-C bonds would be very small. The strong interfacial interaction of small diameter CNTs with the O-terminated Al_2O_3(0001) would be a possible mechanism for the successful Al_2O_3 composite reinforced with CNTs. This phenomena may explain the results of Zhan which states that the increase in fracture toughness is due to the strong bond between CNT and alumina matrix and the existence of crack deflection mechanism.

References

1. Z Xia, L Riester, WA Curtin, H Li, BW Sheldon, J Liang, B Chang, JM Xu, Act Mat. 52(4) (2004), 931-944.
2. J.P.Fan, D.M.Zhuang, D.Q.Zhao, G.Zhang, M.S.Wu, F.Wei, and Z.J.Fan, Appl. Phys. Lett. B. 89, 121910 (2006).

3. G. Yamamoto, M. Omori, T. Hashida, H. Kimura, Nano. 19, 315708 (2008).
4. G. Yamamoto, K. Shirasu, T. Hashida, T. Takagi, J.W. Suk, J. An, R.D. Piner, R.S. Ruoff, Carbon. 49 (2008), 3709-3716.
5. A.G. Evans, J. Am. Ceram. Soc. 73 (1990) 187–206.
6. T. Li, Comput. Sci. Tech. 64 (2004) 2089–2096.
7. J.R. Martinlli, F.F. Sene, Ceram. Int. 26 (2000) 325–335.
8. H. Kawamura, S. Yamamoto, "Improvement of Diesel Engine Startability by Ceramic Glow Plug Start System,", SAE Technical Paper 830580: New York, NY, USA (1983). doi:10.4271/830580
9. W.A. Curtin, B.W. Sheldon, Mater. Today 7 (2004), 44–20.
10. P. Kramer, K. White, Ceram. Eng. Sci. Proc. 3 (1982) 512–518.
11. Y. Tajima, Mater. Res. Soc. Symp. Proc. 287 (1993), 98–201.
12. L. Kumari, T. Zhang, G.H. Du, W.Z. Li, Q.W. Wang, A. Datye, K.H. Wu, Ceram. Int. 35 (2009) 1775–1781.
13. G.D. Zhan, A.K. Mukherjee, Int. J. Appl. Ceram. Technol. 1 (2004) 161–171.
14. W.Orellana, R.H. Miwa and A. Fazzio, Surf. Sci. 566 – 568 (2003) 728–732. http://dx.doi.org/10.1016/j.susc.2004.06.006
15. M. Zhao, W. Xiao, H. Zhang and K. Cho, Chem. Phys., 13, (2011) 11657–11662.
16. M. David, T. Kishi, M. Kisaku, H. Nakanishi and H. Kasai, Jpn. Jour. App.Phys. Vol. 45, No. 4A, (2006). 2869–2871
17. S. Liu et al, CARBON, 49, 3701-3704,(2011)
18. L.L. Li, Z.H.H. Xia, W.A. Curtin, Y.Q.Q. Yang, J Am Ceram Soc 92:10 (2009), 2331–6.
19. B. Huang, Q. Xu, and S.H. Wei, Phys. Rev. B 84, 155406 (2011).
20. W. G. Wyckoff, Crystal Structures 2nd edn (New York: Interscience) (1964).
21. J. Lewis, D . Schwarzenbach, H. D. Flack, Act. Cryst. A38 (1982), 733-739.
22. E .Ziambaras and E .Schroder, Phys. Rev. B. 68, 064112 (2003).
23. R. E. Newnham, Y. M. de Haan, Zeitschrift fur Kristallographie. 117 (1962), 235-237
24. Zhan, G.D., Kuntz, J.D., Wan, J. and Mukherjee, A.K. (2003). Nat. Mat., 2, 38–42.
25. R. Di Felice and J. E. Northrup, Phys. Rev. B 60, 16287(R) (1999).
26. X. G. Wang, A. Chaka, and M. Scheffler, Phys. Rev. Lett. 84, 3650 (2000).
27. Ø. Borck, E. Schroder, J. Phys.: Condens. Matter 18 (2006), 1–12.
28. C. Ruberto, Y. Yourdshahyan and B. I. Lundqvist . Phys. Rev. B 67 195412 (2003)

29. C. Verdozzi, D. R. Jennison, P. A. Schultz and M. P. Sears, Phys. Rev. Lett. 82,799 (1999).
30. K. C. Hass and W. F. Schneider, J. Phys. Chem. B 104, (2000), 5527-5540
31. E. Wallin, J. M. Andersson, E. P. Münger, V. Chirita, and U. Helmersson, Phys. Rev. B 74, 125409 (2006).
32. P. D. Tepesch and A. A. Quong, Phys. Status Solidi B 217, 377 (2000).
33. Z. Lodziana and J. K. Norskov, J. Chem. Phys. 115, 11261 (2001).
34. A. Wander a, B. Searle a, N.M. Harrison, Surf. Sci. 458 (2000), 25–33
35. M. Z.Hossain, Appl. Phys. Lett. 96, 053118 (2010).
36. Y. Sun and Q. Chena. App. Phy. Lett. 95, 021901 (2009)
37. I. D Aditya ,. D. Matsunaka, Y. Shibutani, G. Yamamoto, J. Appl. Phys. 121, 025304 (2017).

Chapter 5 Interfacial Interaction between CNT and Non-oxide Ceramic Material

5.1. Introduction

In the previous chapter, we have found that one of the factors that makes the bond between the CNT and the Al_2O_3 ceramic surface is the oxygen surface which is also the same factor that is responsible for the strong bond between CNT and SiO_2. But howabout nonoxide ceramics material such as SiC, Si_3N_4, Al_4C_3, etc? Since it has no oxygen atoms, can it still have strong interfacial interaction with the CNTs? To answer all of these questions, we analyze interaction between CNT and non-oxide ceramics surfaces.

Non-oxide ceramics include carbides, nitrides, borides, silicides and others have many applications such as superhard abrasives (B_4C, BN) and cutting tools (WC), to rocket nozzles (T_iB_2), electrodes for metal melts (ZrB_2) and heating elements ($MoSi_2$).

TABLE 5. 1 Properties comparison of several ceramic materials[1]

Ceramic	Bonding Atoms	Density (g/cm^2)	Compressive Strength (MPa)	% ionic character	% covalent character
Al_2O_3	Al-O	3.85	2585	63	37
ZrO_2	Zr-O	5.5	1860	73	27
SiC	Si-C	3.1	3860	11	89
Si_3N_4	Si-N	3.19	3450	34.5	65.5

Oxide and non-oxide ceramics properties comparisons are shown in the table 5.1[1]. Due to their high covalent character, non-oxide ceramics have smaller density and not quite as strong as oxide ceramic this is indicated by the higher compressive strength of non-oxide ceramics compared to oxide ceramics. The most important structural non-oxide ceramics are silicon carbide (SiC), silicon nitride (Si_3N_4) . Non-oxides are produced using high temperature processing to reduce inert atmosphere and prevent oxidation in the process. Furthermore, their strength, mostly consisting of covalent (i.e. directional) atomic bonds, inhibits atomic migration (diffusion) so that solid-state sintering below the decomposition temperature (approx. 2500 °C for SiC, approx. 1900 °C for Si_3N_4) is limited. For densification, it needs liquid-phase sintering or reaction-bonding techniques.

Due to its high fracture toughness at both low and high temperatures[2], high thermal conductivity[3,], low chemical reactivity[4], high oxidation resistance[5,6], and very good wear resistance[7], SiC is considered as an good candidate to become the matrix material for Ceramic matrix composites (CMCs). Such fiber-reinforced SiC CMCs are nowadayssuccessfully utilized in various aeronautical and aerospace applications. Reinforcement of SiC matrices with CNTs has been suggested to improve mechanical and functional properties of SiC. Having a wide electronic band gap, SiC is a group-IV polar semiconductor with many potential practical uses in electromagnetic (EM) wave

absorption and shielding applications under harsh oxidative environments[8,9]. The dielectric and electromagnetic properties of SiC powders[10,11], nanofibers[12], foams[13], and SiC matrix composites[14-18] have been the subject of rigorous investigations in the last decade.

Compared to the pure CNT fiber, the CNT-SiC composite-fiber exhibited simultaneously enhanced mechanical properties. This enchanement comes from the high load transfer from SiC to the CNT. As shown in FIG. 5.1, the interface between nanotube and SiC substrate is clean and the load transfer is highly possible. They expect that the strong bonding between SiC and CNT will occur[18,19].

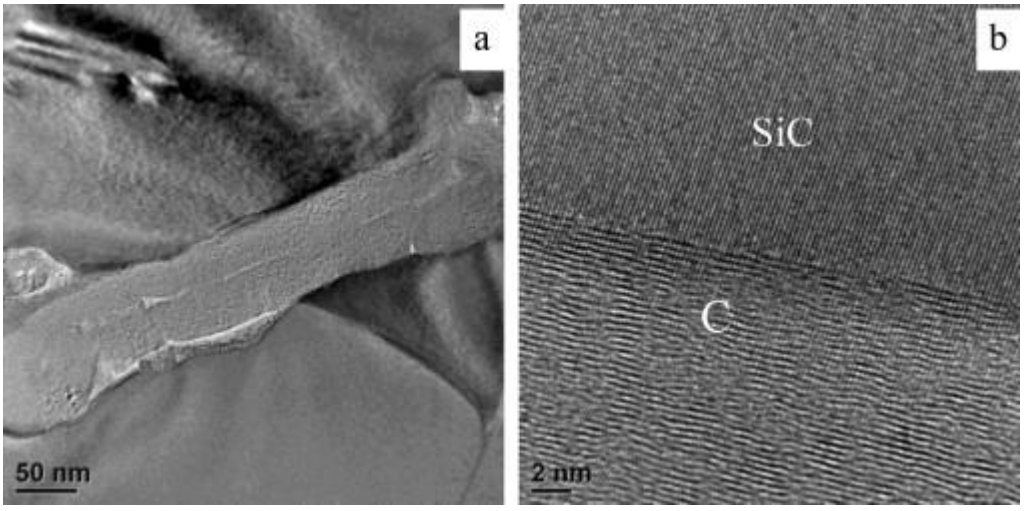

FIG. 5. 1 TEM micrographs with a) low and (b) high magnification images showing the clean interface between MWCNT and SiC for SiC–0.5 mass % MWCNTs samples (Figure 6 of Ref. 19).

Unfortunately, the experimental results show that there is no significant increase of fracture toughness on CNT non-oxide ceramic composites as shown in the following table:

TABLE 5. 2 Mechanical properties of CNT-SiC composites by Ma[20] and CNT-Si_3N_4 composites Balaszi[21].

Materials	Relative Density (%)	Bending Strength (MPa)	Fracture Toughness (MPa $M^{1/2}$)
SiC	93.9	317.5	3.47
SiC + 10% CNT	94.7	348.5	3.84
Materials	Relative Density (%)	Vickers microhardness (GPa)	Fracture Toughness (MPa $m^{1/2}$)
Si_3N_4	3.23	20.1	5.2
Si_3N_4 + 1% MWNT	3.17	16.6	5.3

Ma notes that this insignificant increase is due to the inadequate interaction between CNT and SiC matrices with a fixed crack deflection at the interface between CNT and the surface of the SiC matrix. Therefore, a major aim of this work is to investigate effects of the CNT diameter to the interfacial interaction between CNTs and nonoxide ceramic surface namely SiC (0001) using first-principles calculations based on the density functional theory (DFT). Advance in a DFT approach means it is now possible to describe the interfacial interaction between CNTs and surfaces with the detail and accuracy required for computational results.

5.2 Results and Discussions

A. SiC Bulk and Surface

The basic structural element of SiC crystals is a hexagonal bilayer containing silicon and carbon in alternating positions. We compare our calculated results of bulk

SiC with experimental results and previous theoretical calculations which also used GGA-PBE.

TABLE 5. 3 Comparison of the unit vectors *a*, *b* and *c* of Bulk SiC calculation with reference[25]

Ceramics Material	*Space Group*	This work (Å)			*References* (Å) [22]					
					Experiment (Å)			*Calculation* (Å)		
		a	*b*	*c*	*a*	*b*	*c*	*a*	*b*	*c*
SiC	*Hexagonal* (C^4_{6v}-$P6_3mc$)	3.077	3.077	15.11	3.073	3.073	15.118	3.09	3.09	15

From TABLE 5.3, we notice that PBE functional we use makes the accurate estimates of equilibrium lattice parameters of SiC consistent with experimental values, it overestimates the lattice constants only by ~0.13% .

In this study, we consider two kinds of surface terminations of SiC surface. Both of Si- and C-terminated surfaces are nonstoichiometric. The Si-terminated SiC(0001) surface model has four Si layers and three C layers, while the C-terminated SiC(0001) surface model contains four C layers and three Si layers, and thus each surface system is consisting of 126 silicon and carbon atoms with a 40 Å vacuum region. The bottommost atoms in both models have the broken bonds terminated by hydrogen atoms.

Our surface relaxation calculation of SiC surfaces showed that the distance of Si layer and C layer was 1.91 Å and the distance between two nearest Si layers was 2.52 Å after relaxation. These results match with the report by Capitani et.al[23] which mentions that the distance between Si layer and C layer after relaxation is around 1.89 Å and the distance between two nearest Si layers is 2.52 Å. Both values are much close each other.

B. Adhesion behavior of CNT/SiC(0001) Interface

We studied the interface interaction of the CNTs on the SiC (0001) since (0001) surface is well-known as the most stable surface for hexagonal SiC. We considered both Silicon (Si-) and Carbon (C-) surface terminations of SiC(0001). To investigate the interfacial interaction of CNTs and SiC, we calculated the system in the tetragonal cell. In our models, the axial direction of the CNTs is set to be parallel to $[10\bar{1}0]$ on the SiC(0001) (see FIG.5.2(a)). The interface model consists of the CNT and SiC surface with dimensions of 9.23 Å and 15.99 Å. The difference between tetragonal SiC cell size and CNT length provides the interface lattice mismatch of about 8.3%. The CNT was strained and the SiC was kept to its equilibrium lattice constant because the SiC matrix is hard to deform compared with CNT due to the quite large difference of their rigidities.

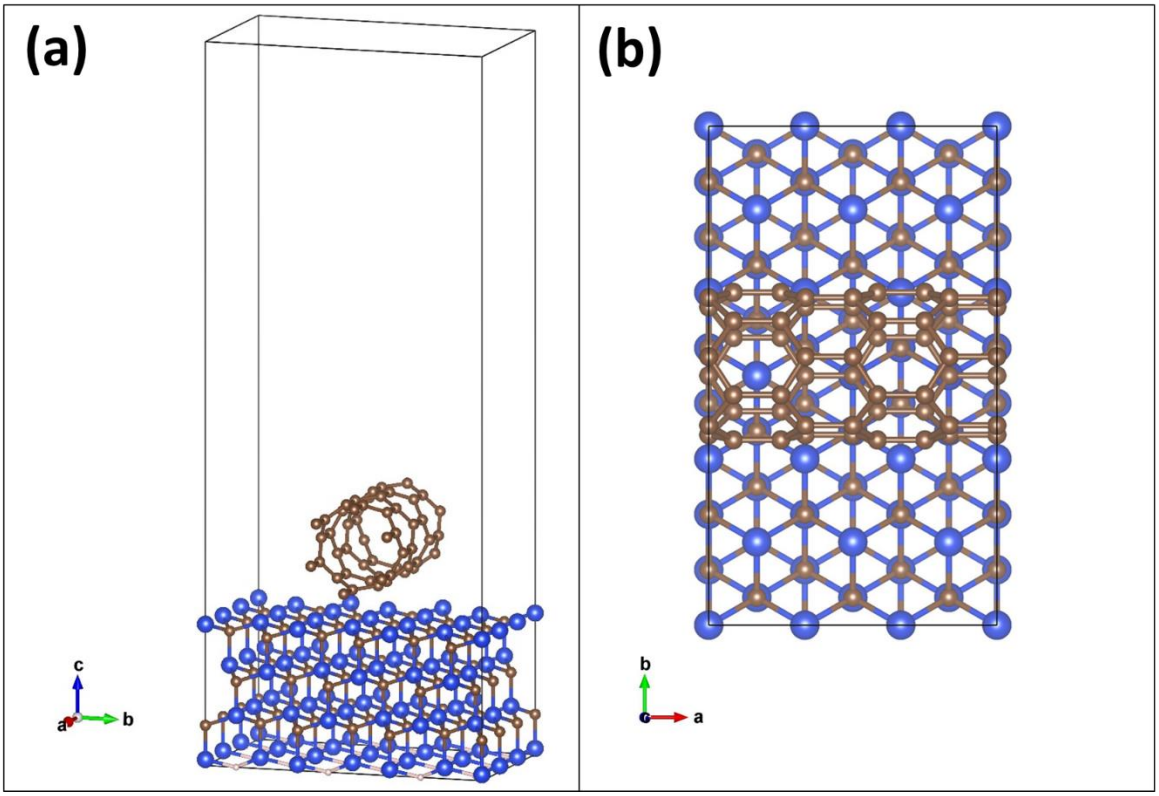

FIG. 5. 2 Side (a) and top (b) views of CNT on SiC (0001). The brown and blue balls denote the C and Si atoms, respectively. The black lines represent the unit cell in calculations[25].

As an interfacial configuration between CNT and SiC(0001), we considered different initial adsorption sites, where a surface Si or C atom of SiC was directly below either at the position of C atom of the CNT, at the hollow site of the CNT or at the center of the C-C bridge site. Additionally, we also evaluated the arrangements where the lowermost C atom of CNT was directly above either the hollow site of Si-C surface atoms or the Si-C bridge site of surface atoms. The difference of the charge density is calculated to investigate the CNT–surface interfacial bonding using Eq.4.1 (see Appendix C).

As depicted in FIGs.5.3 (a) and (f), the smallest diameter CNT of (3,0) was relaxed into an arch-like structure on both of Si- and C-terminated SiC surfaces. which is the same structural change as the previous CNT-Al_2O_3 case in ref. 25. This adsorbing process involving spontaneous dissociation of C-C σ bonds of the CNT implies that the Si- and C-terminated SiC surfaces have some catalytic effect, and the activation energy barrier for the bond breaking would be vanishingly small. Such geometrical transformation to an arch-like structure has occured for the (3,0) CNT on O-terminated Al_2O_3(0001) as the previous first-principles calculation of CNTs on Ni performed by David et al[24]. On the other hand, for the larger diameter CNTs of (6,0), (9,0), (12,0) and graphene, the change of the structures is relatively small compared with the smallest diameter CNT. Local charge accumulation is observed between the C atoms of the CNTs and Si atoms of the Si-terminated surface, indicating that the interfacial C-Si bonds have covalent characteristic. Additionally, FIG.5.3 also displays charge

depletion around the Si atoms of SiC surfaces near the CNTs, which corresponds to ionization of the Si atoms donating electrons to C atoms of the CNT.

On the other hand, for the C-terminated surface, charge accumulation can also be seen between the C atoms of the CNTs and the C-terminated surface, while the charge depletion is surrounding at the interfacial C atoms of the CNT for the smallest diameter CNT case and C atoms of the C-terminated surface. Thus, these results give rise to the covalent and ionic characteristics in the interfacial C-C bonds.

Isosurface level of the charge density difference for the Si-terminated surface is larger than for the C-terminated surface, indicating the stronger bonding between CNT and Si-terminated surface. It can also be seen from the structural changes of the CNT on the Si-terminated surface more significantly than on the C-terminated surface.

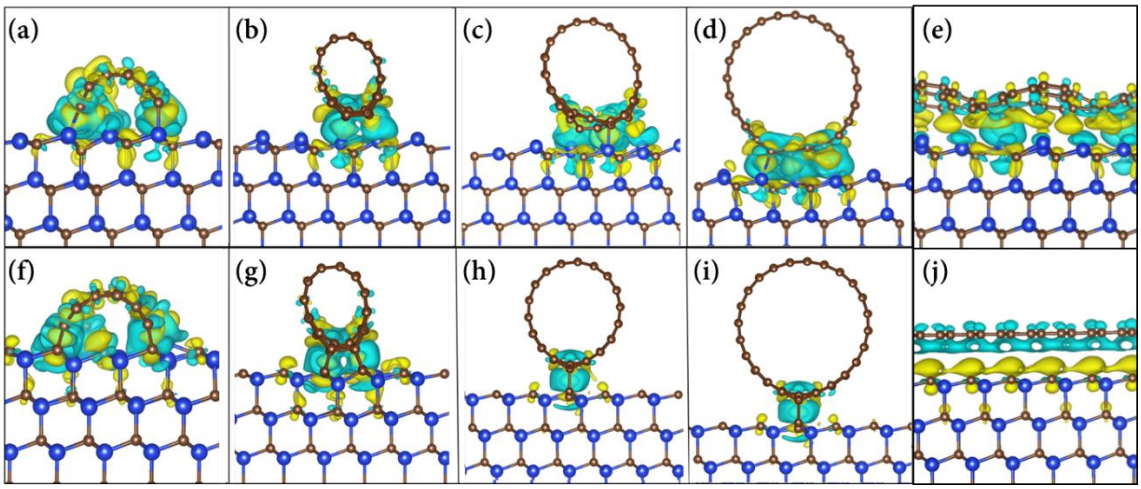

FIG. 5. 3 Calculated charge density difference for the most stable configurations about (a) (3,0), (b) (6,0), (c) (9,0), (d) (12,0) CNTs, (e) graphene on Si-terminated SiC(0001), and (f) (3,0), (g) (6,0), (h) (9,0), (i) (12,0) CNTs, (j) graphene on C-terminated SiC(0001), respectively. Color key: brown and blue denote the C and Si atoms. Isosurface level for (a)-(d) and (f)-(i) are 0.0025 $e^{-}/Å^{3}$, and (e) and (j) are 0.0015 $e^{-}/Å^{3}$ and 0.0005 $e^{-}/Å^{3}$. Isosurfaces charge densities in yellow indicates accumulation in charge density, while blue indicates depletion.[25]

C. Interface structures and bonding of CNT/SiC (0001)

The adhesion energy of CNTs on the Si-terminated surface slightly stronger than on the C-terminated surface. The qualitative trend of the adhesion energy correlates to the interfacial interatomic distances and the charge density difference of the CNT/SiC interfaces.

The adhesive energy is qualitatively consistent with the charge density difference. The adhesive energy of CNTs on stoichiometric surfaces is relatively weaker (see dashed lines of Al-terminated Al_2O_3(0001) in FIG.5.4) being compared with the nonstoichiometric surfaces (see solid lines of O-terminated Al_2O_3(0001), Si-terminated SiC(111), C-terminated SiC(111) in FIG.5.4). The adhesive energy of the smallest diameter CNT (3,0) is always much stronger on the nonstoichiometric surfaces compared with the other cases because of the strong bonding of the dissociated C atoms of the CNT with the nonstoichiometric surfaces. Adhesive energy of the graphene-ceramic interface is not much different from one another (see "∞" at the horizontal axis in FIG.5.4). It shows that for large diameter CNTs, their interface would have almost the same interfacial strength regardless of the kind of ceramics.

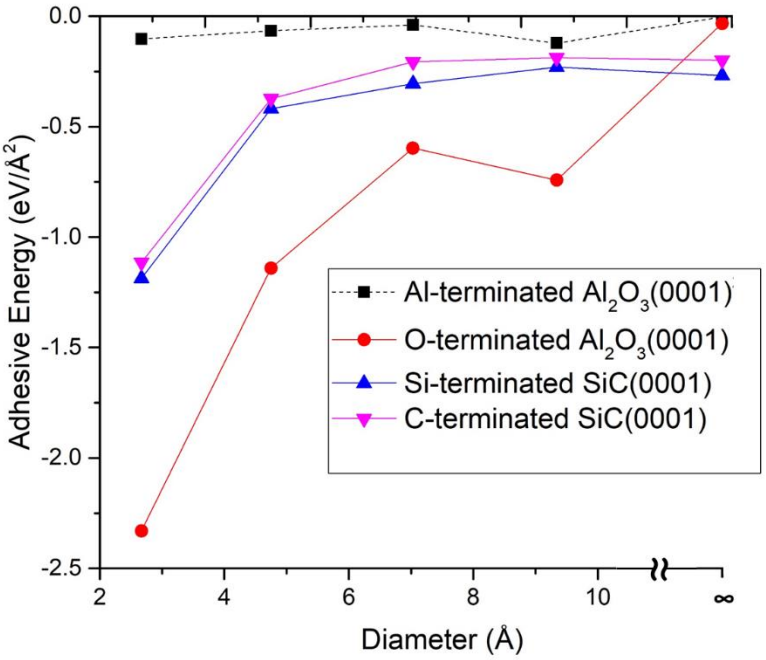

FIG. 5. 4 Adhesive energy as a function of CNT diameter

From FIG.5.3 we can see that interfacial bonds of CNT/SiC(0001) exhibits a mixture of covalent and ionic bonding. In order to obtain a quantitative measure of the covalent bond strength, the integrated COHP values (ICOHPs) up to E_F of selected interatomic contacts are calculated, and the Bader analysis is used to analyze the ionic characteristic in the interaction between CNTs and ceramic surfaces.

Adhesive energies of CNTs and Si-terminated SiC(0001), C-terminated SiC(0001) in FIG. 5.4 have almost the same values but the bonding characters are different. The covalent interaction between CNTs and C-terminated SiC(0001) is much higher than that of Si-terminated surface SiC(0001). On the other hand, Si-terminated SiC(0001) have the stronger ionic character at the interface compared with C-terminated SiC(0001), which indicates that they have the more active charge transfer.

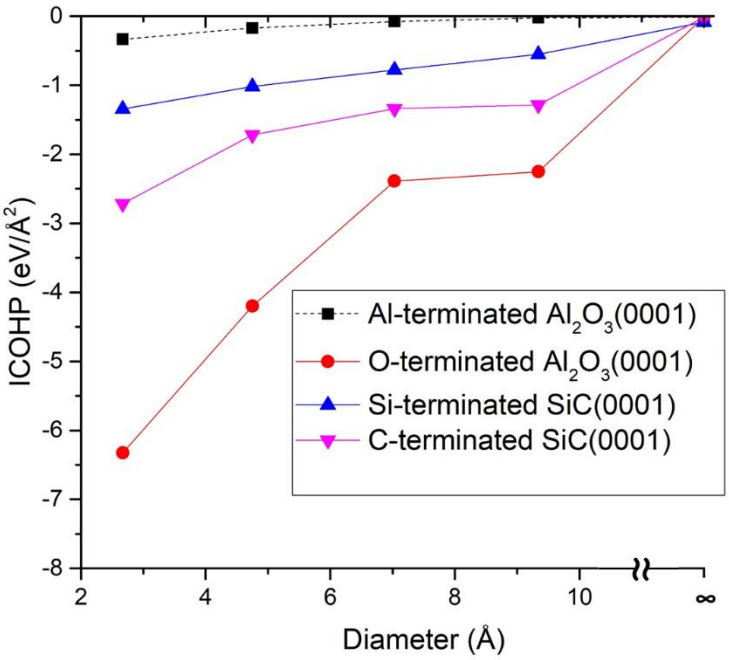

FIG. 5. 5 ICOHP as a function of CNT diameter.

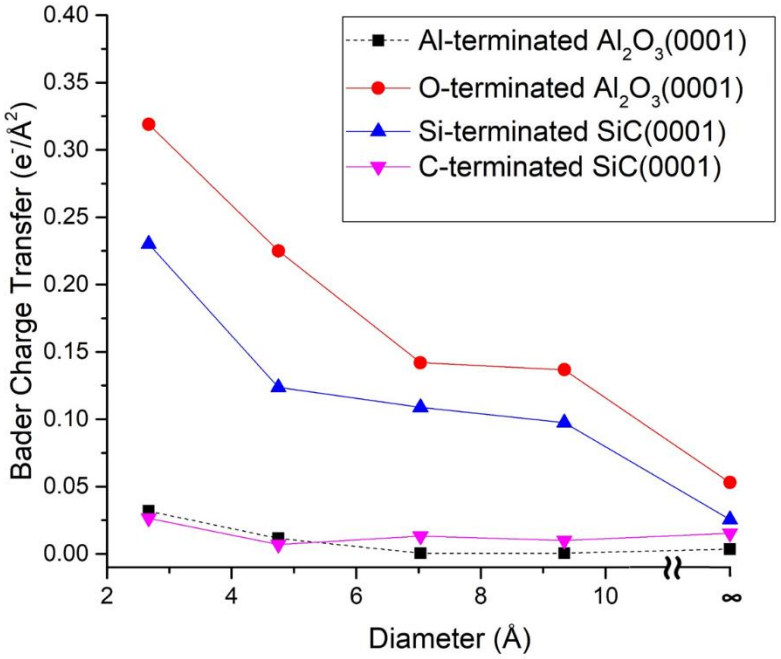

FIG. 5. 6 Charge transfer as a function of CNT diameter.

These covalent and ionic properties of the interface are important because they affect the way how a crack propagates on the interface. Several works have successfully demonstrated the effect of the bonding type on the resistance to crack propagation. The directional covalent bond is expected to provide a favorable condition for bond trapping of cracks. Meanwhile, ionic bond would probably show the less bond trapping effects[26-30].

The results shown in Figs 5.5 and 5.6 could give us some insights about the nature of the interface properties from their relationship to the experimental results obtained in TABLE 5.2, where the fracture toughness of several CNT-ceramic composites are summarized.

The smaller increase in fracture toughness of the CNT-SiC composites when compared with CNT-Al_2O_3 composites might be due to the inadequate covalent characteristic between CNTs and C- and Si-terminated SiC(0001) surfaces when compared to CNTs with O-terminated Al_2O_3(0001) (see Fig. 5.5). Since the covalent characteristic at the interface between CNT and C-terminated SiC (0001) is more dominant compared with the ionic characteristic, thus the interface resistance to the crack growth could be expected. This may further assist the prevention of crack propagation, possibly increasing the composite's fracture toughness as shown in TABLE 5.2. However, the fracture toughness is slightly improved because the covalent character is lower than the case of CNT and O-terminated Al_2O_3(0001).

5.3 Conclusion

In this study, we investigated the interfacial interaction of CNT/SiC(0001) using first-principles calculations. On the nonstoichiometric surfaces, i.e. Si- and C-terminated SiC surfaces, the structure of all CNTs changed depending on the diameter.

On stoichiometric ceramic surfaces, namely the Al-terminated Al_2O_3, the structure of all the CNT with any diameter did not drastically change from that before adsorbing and the adhesive energy per contact area was weak. On the other hand, for the nonstoichiometric surfaces, i.e. Si- and C- terminated SiC surface, the bond breaking of the CNT with (3,0) was occurred and it shows the strong diameter dependence. The small diameter CNT has a strong interaction with the nonstoichiometric surfaces, caused by the opening of CNTs and the successive geometrical transform into an arch-like structure. This behavior means that the nonstoichiometric surfaces has a catalytic effect and the activation energy barrier for dissociation of C-C bonds would be very small.

The interfacial interaction between CNTs and ceramic surfaces has the mixed covalent-ionic nature which is quantitatively measured by the ICOHP and Bader analyses. The fracture toughness CNT-SiC composite is slightly improved because the covalent character is lower than the case of CNT and O-terminated Al_2O_3(0001).

References

1. W. F. Smith, J. Hashemi., Foundations of Materials Science and Engineering, Published by McGraw-Hill, 4th Ed., (2006).
2. M. Keppeler, H. G. Reichert, J. M. Broadley, G. Thurn, I. Wiedmann, F. Aldinger. J Eur Ceram Soc 18:521–526 (1998)

3. H. Nakano, K. Watari, Y. Kinemuchi, K. Ishizaki, K. Urabe. J Eur Ceram Soc 24:3685–3690 (2004)
4. L. S. Sigl. J Eur Ceram Soc 23:1115–1122 (2003)
5. P. Greil. Advanced Engineering Ceramics. Adv Eng Mater 4:247–254 (2002)
6. F. Rodrı´guez-Rojas, A.L. Ortiz, F. Guiberteau, M. Nygren. J Eur Ceram Soc 31:2393–2400 (2011).
7. J. A. Costello, Tressler RE. J Am Ceram Soc 64:327–331 (1981)
8. S. Lafon-Placette, K. Delbe´, J. Denape, M. Ferrato. J Eur Ceram Soc 35:1147–1159 (2015)
9. T. Razzaq, J. M. Kremsner, C.O. Kappe. J Org Chem 73:6321–6329 (2008)
10. W.L.E. Wong, M. Gupta. Microwave and metals. Wiley, Singapore (2007)
11. D.L. Zhao, F. Luo, W.C. Zhou. J Alloys Compd 490:190–194 (2010)
12. B. Zhang, J. Li, J. Sun, S. Zhang, H. Zhai, Z. Du. J Eur Ceram Soc 22:93–99 (2002)
13. R. Wongmaneerung, P. Singjai, R. Yimnirun, S. Ananta. J Alloys Compd 475:456–462 (2009)
14. H. Zhang, J. Zhang, H. Zhang. Compos Part A Appl S 38:602–608 (2007).
15. X. Li, L. Zhang, X. Yin, L. Feng, Q. Li. Scr Mater 63:657–660 (2010).
16. X.M. Yu, W.C. Zhou, F. Luo, W.J. Zheng, D.M. Zhu. J Alloys Compd 479:L1–L3 (2009)
17. H. Mei, D. Han, S. Xiao, T. Ji, J. Tang, L. Cheng. Carbon 109:149–153 (2016)
18. X. S. Zhang , L. W. Yang, H. T. Liu and M. Zu. *RSC Adv.*, **7**, 23334-23341 (2017)
19. D. Jiang ,. J. Zhang, Z. Lv,. J. Eur. Ceram. Society 32, 1419–1425 (2012)
20. R.Z. Ma, J. Wu, B.Q. Wei, J. Liang, and D.H. Wu,. J. Mat. Sci., 33, 5243–5246 (1998).
21. C. Balazsi, Z. Shen, Z. Konya, Z. Kasztovszky, F. Weber, Z. Vertesy, L.P. Biro, I. Kiricsi, and P. Arato, Comp. Sci. and Tech., 65, 727–733 (2005).
22. N.M. Caffrey, R. Armiento, R. Yakimova, and I.A. Abrikosov, Phys. Rev. B 92, 081409(R) (2015)
23. G. C. Capitani, S. di Pierro, and Gioacchino, Temp. Am. Min., Volume 92, 403-407, (2007).
24. M. David, T. Kishi, M. Kisaku, H. Nakanishi and H. Kasai, Jap. J. App. Phys. Vol. 45, No. 4A, (2006). 2869–2871

25. I. D Aditya, D. Matsunaka, Y. Shibutani, Suprijadi, AIP Adv. (2018) Under reviewing process.
26. G. schoeck, W. Pich: Phys.stat.sol. 118 (1990) 109-115.
27. P. Gumbsch, R. Cannon: MRS Bulletin, 25(5) (2000) 15-20.
28. J. E. Sinclair: Phil. Mag. 31(3) (1975) 647-671.
29. K. W. K. Leung, Z. L. Pan, D. H. Warner. Modell. Simul. Mater. Sci. Eng (24) (2016) 035004.
30. E. Bitzek, J.R. Kermode, P. Gumbsch: Int. J. Fract. 191 (2015) 13–30.

Chapter 6 Interfacial Interaction between CNT and Oxide-ceramic Materials with Stoichiometric Oxygen Terminated Surface

6.1. Introduction

In the previous two chapters we have known that the terminated oxygen surface of Al_2O_3 has an important role in the interaction between CNT and Al_2O_3 whereas after studying the intraction between CNTs and non-oxide ceramic, namely SiC, we know that nonstoichiometric surfaces have stronger bonds with CNTs than stoichiometric surfaces. To confirm these two factors, we selected ZrO_2(111) which has an O-terminated surface as a stoichiometric surface. From this calculation we hope to know which factors are more dominant between the stoichiometry of the surfaces or the oxygen atoms that interact with CNTs resulting in strong bonds between CNTs and ceramics.

Like SiC, zirconia (ZrO_2) is a specific material with high potential to be used in ceramic materials, due to its high ionic and thermal conductivity, in addition to mechanical properties. ZrO_2 is a white crystalline oxide of zirconium. It can occur

naturally or synthesized in three main phases: monoclinic, tetragonal, and cubic. In addition, zirconia is chemically unreactive. Under higher temperatures, ZrO_2 adopts a tetragonal and cubic structure. ZrO_2 particles are used as one of the most common fillers, leading to an increase in fracture toughness and chemical inertness. Recent studies suggest that the mechanical properties of CNCs with ZrO_2 could be considerably increased by reducing the level of grain size and by achieving high levels of dispersion of these particles in the matrix.

A lot of works has been devoted to designing and synthesizing zirconia and its composites; however, few studies involve ZrO_2-CNT composites. Rao et al.[1] managed to fabricate hollow nanotubes of zirconia using CNTs as templates. Javey et.al[2] have worked on integration of ZrO_2 and SWCNTs by forming ZrO_2 thin-films on top of individual SWCNTs and used as gate dielectrics for nanotube field-effect transistors. More recently, Shan and Gao[3] synthesized ZrO_2-CNT composites by hydrothermal treatment of multiwalled carbon nanotubes (MWNTs) in $ZrOCl_2,8H_2O$ aqueous solution at 150 °C. Sun et al[4] has shown that there is clean interface between CNT and ZrO_2 which indicate load transfer is highly possible and strong bonding between ZrO_2 and CNT may occurs.

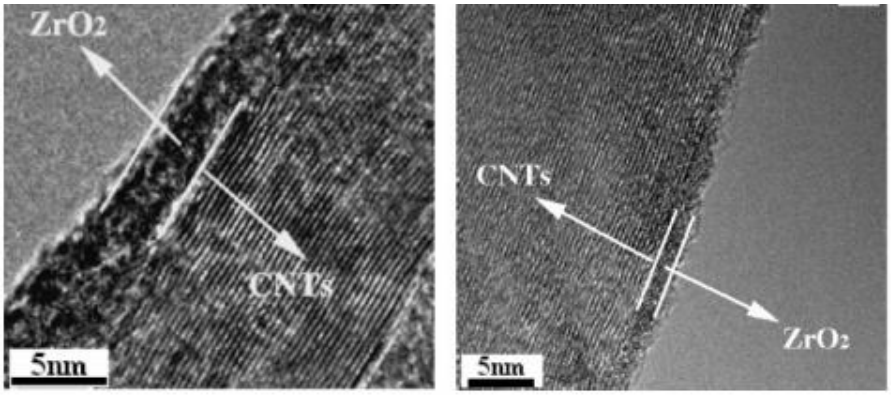

FIG. 6. 1 TEM micrographs showing the clean interface between CNT and ZrO_2[4]

Unfortunately, the experimental results show that the fracture toughness of ZrO_2 after CNT added decreases as shown in the following result by Kasperski[5]:

TABLE 6. 1 Mechanical properties of CNT-ZrO_2 composites by Kasperski[5]

Materials	Relative Density (%)	Vickers microhardness (GPa)	Fracture Toughness (MPa $m^{1/2}$)
ZrO_2	98	13.8	10.3
ZrO_2 + 1.2% CNT	≈100	12.3	7.1
ZrO_2 + 1.7% CNT	99	11.7	6.6
ZrO_2 + 4.5% CNT	98	10.0	5.5
ZrO_2 + 6.3% CNT	96	9.5	5.1

Kasperski's work results show that for composite CNT-ZrO_2 does not show any increase in fracture toughness. This is due to weak interfacial bonding between CNTs with ZrO_2 and also no crack deflection on this composite. This chapter aims to find out further why the fracture toughness of CNT-ZrO_2 composites dercreased by studying the interfacial interaction interaction between CNTs and ZrO_2 surfaces.

6.2 Result and Discussion

A. ZrO_2 Bulk and Surface

As ceramics materials, we investigate in this work ZrO_2. In TABLE 6.2., we compare our calculated results of these ceramics with experimental results and previous theoretical calculations which also used GGA-PBE.

TABLE 6. 2 Comparison of the unit vectors *a*, *b* and *c* of Bulk SiC and ZrO_2 calculation with references[12]

Ceramics Material	*Space Group*	This work (Å)			*References* (Å) [6]					
					Experiment (Å)			*Calculation* (Å)		
		a	*b*	*c*	*a*	*b*	*c*	*a*	*b*	*c*
ZrO_2	*Cubic (Fm3m)*	5.127	5.127	5.127	5.086	5.086	5.086	5.13	5.13	5.13

From Table 6.1, we notice that our result on lattice parameter of ZrO_2 is in good agreement with experimental values. For PBE overestimate the lattice constants only by ~0.8%. Starting from the ZrO_2 relaxed bulk structure, we created slab models representing the stoichiometric (111) surface (O-terminated) using two Zr layers and four O layers with a 40 Å vacuum region in a tetragonal cell. The atomic structure of the nonstoichiometric (Zr-terminated) systems is constructed by using three Zr layers and four O layers. After surface relaxation, the interplanar distance of first and second layers of the surface increased by 7.5% compared to the bulk structure which is in a good agreement with the reference.[7]

B. Adhesion behavior of the CNT/ZrO_2(111) Interface

In our models, the axial direction of CNT is set to be parallel to $[11\bar{2}0]$ on ZrO_2(111) (see FIG.6.2). The interface models constructed by placing the CNT above ZrO2(111) unit cells with dimensions of *a*= 21.75 Å and *b*=12.56 Å. The lattice parameter of ZrO_2 as a matrix in the models is fixed due to the same reason as CNT-SiC. Therefore, the CNT along the axial direction is stretched by 0.10 Å per cell of the model (i.e. axial strain of 0.82%).

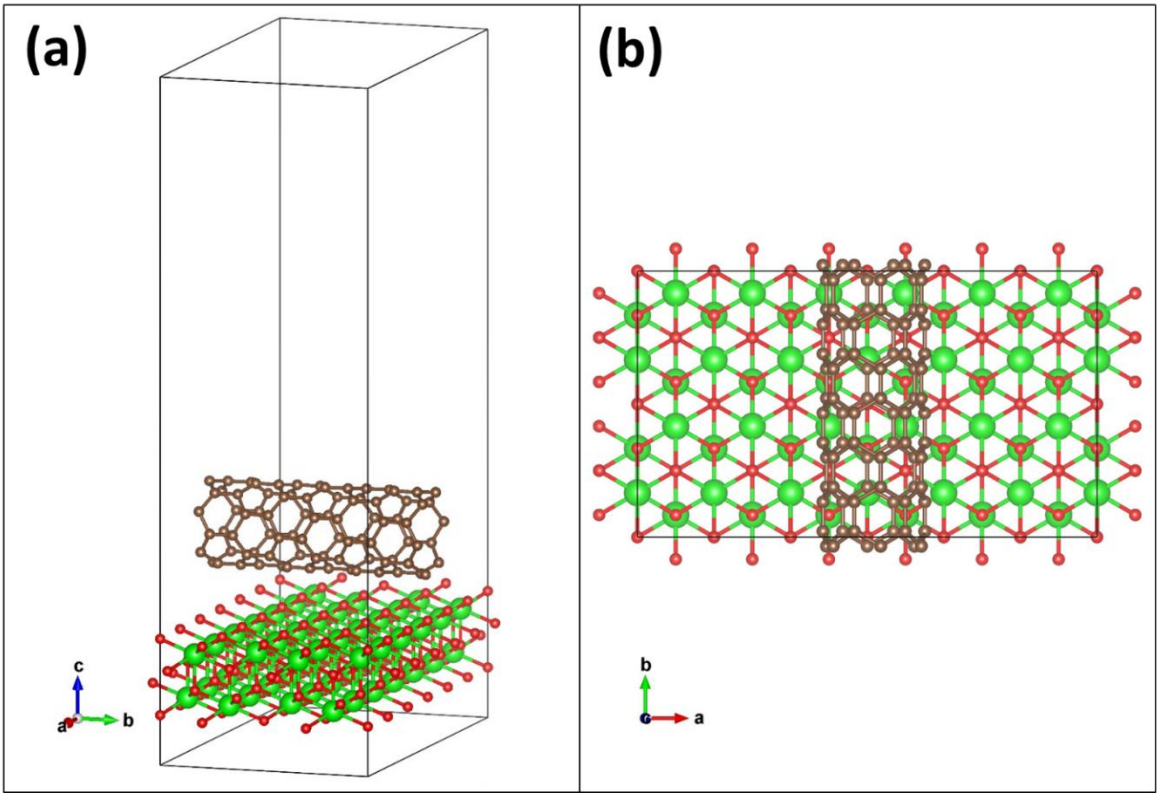

FIG. 6. 2 Side (a) and top (b) views of CNT on ZrO_2(111). The brown, green, and red balls denote the C, Zr, and O atoms, respectively. The black lines represent the unit cell in calculations.[12]

As an interfacial configuration between CNT and the ZrO_2(111), we considered different initial adsorption sites where a surface Zr or O atom was directly below either a C atom of the CNT, at the hollow site of CNT or at the center of the C-C bridge site. Additionally, we also evaluated the other arrangement where the lowermost C atom of CNT was directly above either the hollow site of surface atoms or the bridge site of surface atoms (Appendix C).

The structures of CNTs and O-terminated ZrO_2(111) (stoichiometric surface) hardly change from those before adsorbing through relaxation, as shown in Figs. 2 (a) to (d) which show the difference of charge transfer in CNT-ZrO_2(111) surface. The same behavior can also be encountered on CNT/Al-terminated Al_2O_3(0001) where the

suface structure was relaxed keeping the stoichiometric configuration 23). The isosurface level of CNTs and O-terminated ZrO_2 (111) is lower than that of Zr-terminated surface, indicating the weaker interaction between CNTs and O-terminated surface. Local charge density accumulated between C atom of the CNT and O atom of the ZrO_2 surface represents a covalent bonding between atoms. Additionally, surrounding charge depletion shows that it has not only covalent but also ionic characteristics due to the charge transfer from the O-terminated surface. Compared among FIGs. 6.3 (a) to (d), we can see that the (3,0) CNT/O-terminated surface ZrO_2 has higher charge density difference than the larger CNTs. It shows that the interaction of the smallest diameter CNT with the O-terminated ZrO_2(111) is much stronger than the large diameter CNTs.

Unlike the O-terminated surface, the smallest diameter CNT of (3,0) was relaxed into an arch-like structure on the Zr-terminated surface, as shown in FIGs. 6.3 (f) to (i), while the larger diameter CNTs slightly changed from that before adsorption. This proves that the geometrical transformation of CNT into an arch-like structure occurs only when the CNT interacts with the nonstoichiometric surface. The mixed ionic-covalent characteristic, found in the interaction between CNTs and the Zr-terminated ZrO_2 surface with the accumulated charge between Zr and C atoms and charge depletion from Zr atoms, shows the charge transfer from the surface. The obtained results imply that the interaction of CNT with ceramics gives rise to a catalytic effect on the C-C bond breaking, depending on the CNT diameter and the stoichiometry of ceramic termination. This adsorbing process involving spontaneous dissociation of C-C σ-bonds shows that the Zr-terminated ZrO_2 (111) has a catalytic effect and the activation energy barrier for the bond breaking would be vanishingly small this supports what has been shown in David's study results[9].

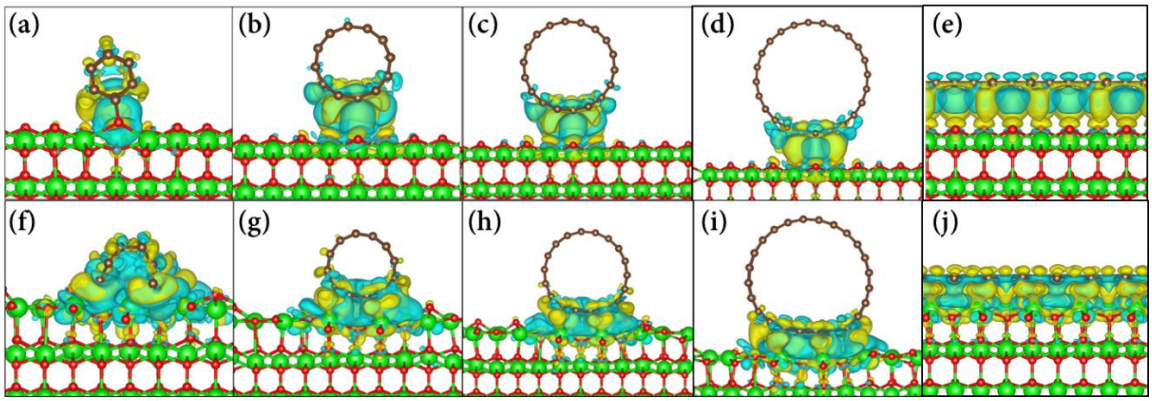

FIG. 6. 3 Calculated charge density difference for the most stable configuration about (a) (3,0), (b) (6,0), (c) (9,0), (d) (12,0) CNTs, (e) graphene on O-terminated $ZrO_2(111)$, and (f) (3,0), (g) (6,0), (h) (9,0), (i) (12,0) CNTs, (e) graphene on Zr-terminated $ZrO_2(111)$, respectively. Color key: brown, light green and red denote the C, Zr and O atoms, respectively. Isosurface levels for (b), (c), (d) and (e) are 0.00011 $e^-/Å^3$ and the others are: 0.0015 $e^-/Å^3$. Isosurfaces charge density in yellow indicates accumulation in charge density, while blue indicates depletion.[12].

C. Interface structures and bonding CNT/ZrO_2 (0001)

To quantitatively analyze the interfacial interaction of CNT and the ceramic surfaces, the adhesive energy per projected contact area is calculated using Eq.4.2. The calculated adhesive energy results are showed as a function of the CNT diameter, in FIG. 6.4. For reference, the results for CNT/Al_2O_3 and CNT/SiC calculated in our previous chapter are also included.

The adhesive energy is qualitatively consistent with the charge density difference. The adhesive energy of CNTs on stoichiometric surfaces is relatively weaker (see dashed lines of Al-terminated $Al_2O_3(0001)$, O-terminated $ZrO_2(111)$ in FIG.6.4) being compared with the nonstoichiometric surfaces (see solid lines of O-terminated $Al_2O_3(0001)$, Si-terminated SiC(111), C-terminated SiC(111), Zr-terminated $ZrO_2(111)$ in FIG. 6.4). The adhesive energy of the smallest diameter CNT (3,0) is always much stronger on the nonstoichiometric surfaces compared with the other cases

because of the strong bonding of the dissociated C atoms of the CNT with the nonstoichiometric surfaces. Adhesive energy per contact area for the graphene-ceramic interface is not much different from one another (see "∞" at the horizontal axis in FIG.6.4). It shows that for large diameter CNTs, their interface would have almost the same interfacial strength regardless of the kind of ceramics.

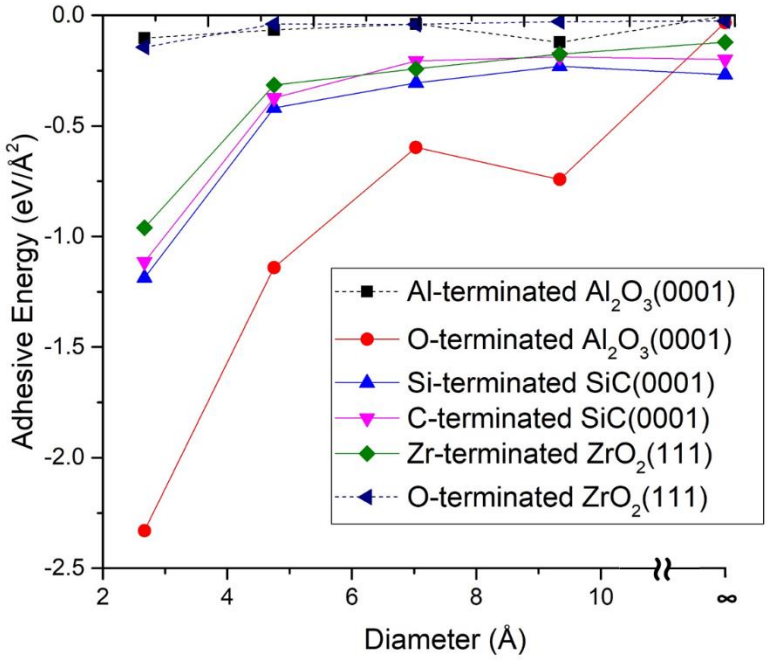

FIG. 6. 4 Adhesive energy as a function of CNT diameter[12].

Results of ICOHP analyses in FIG. 6.5 and Bader analyses in FIG. 6.6 support and elucidate our results on the adhesive energy for each interaction between CNTs and ceramic surfaces. For example, the strongest adhesive energy of the combination of CNTs and O-terminated Al_2O_3 comes from both strong covalent and ionic bonding between C atoms of the CNT and O atoms of surface. It can be seen that the values of ICOHP are roughly inversely proportional to CNT diameter, i.e., the negatively larger ICOHP value corresponds to the smaller diameter CNT and possible stronger covalent

interaction. Bader charge transfer results also show that the smaller diameter CNT has the stronger ionic character with the higher charge transfer.

Adhesive energies of CNTs and Si-terminated SiC(0001), C-terminated SiC(0001) and Zr-terminated ZrO_2(111) in FIG.6.5 have almost the same values but the bonding characters are different. The covalent interaction between CNTs and C-terminated SiC(0001) is much higher than that of Si-terminated surface SiC(0001) and Zr-terminated ZrO_2(111). On the other hand, Si-terminated SiC(0001) and Zr-terminated ZrO_2(111) have the stronger ionic character at the interface compared with C-terminated SiC(0001), which indicates that they have the more active charge transfer.

The adhesive energy in the interaction between CNT and Zr-terminated ZrO_2(111) is almost similar to that when CNT interacts with SiC. It might be understood that the bond between CNT and ZrO_2 is still strong enough. However, the decrease in fracture toughness of CNT-ZrO_2 composite in Table 6.1 is due to the relatively smaller covalent bond characteristic and also to the larger ionic bond characteristic observed at the interface between CNT and Zr-terminated ZrO_2. These bond states of CNT-ZrO_2 composite make a crack easier to propagate along the interface, and as a result, the decrease of fracture toughness might be happened as seen in Table 6.1.

Above all else, the covalent characteristic at the interface between CNT and O-terminated Al_2O_3(0001) surface is much greater compared with that when CNTs interact with the other ceramic surfaces. It may lead to the significant increase of fracture toughness than the other ceramic composites for almost twice of Al_2O_3 without CNT.

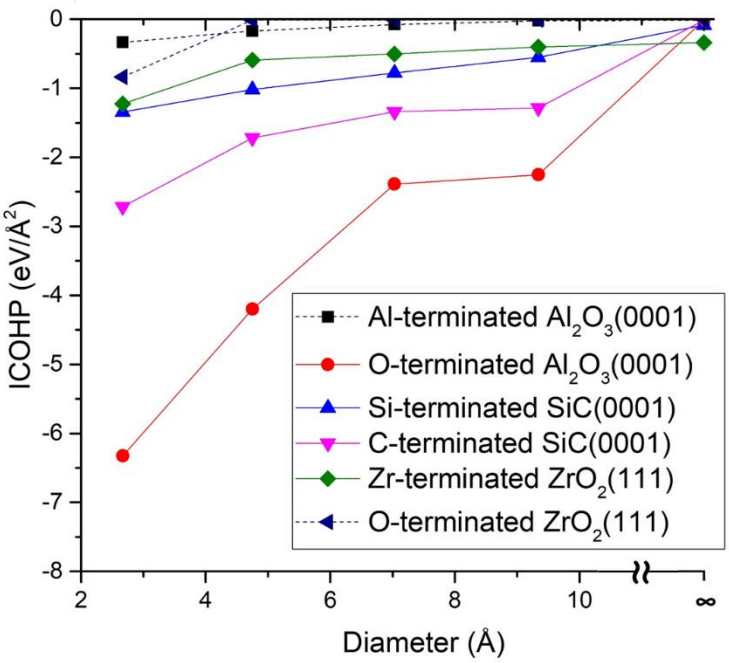

FIG. 6. 5 ICOHP as a function of CNT diameter[12].

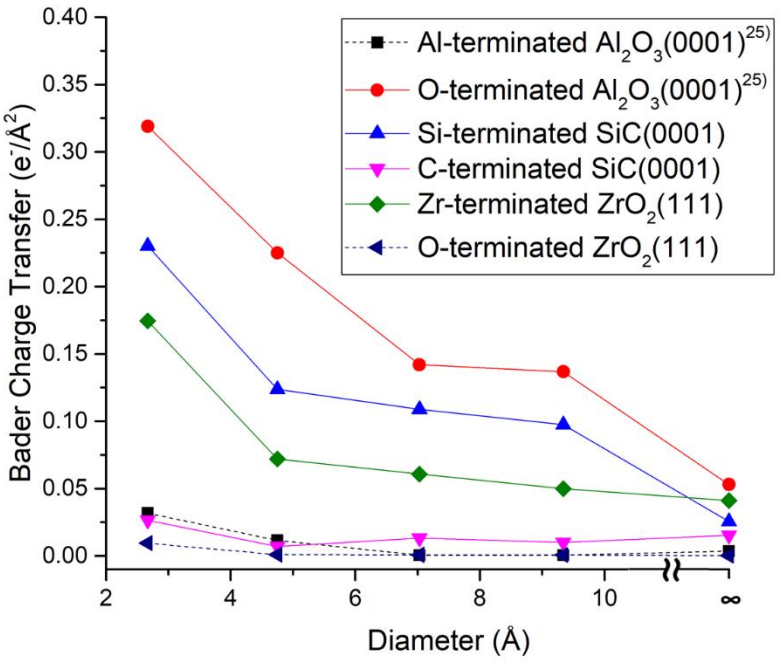

FIG. 6. 6 Charge transfer as a function of CNT diameter[12].

6.3 Conclusion

In this chapter, we investigated the interfacial interaction of CNT-ZrO_2(111) using first principle calculations. On stoichiometric ceramic surfaces, namely the O-terminated ZrO_2(111), the structure of all the CNT with any diameter did not drastically change from that before adsorbing and the adhesive energy per contact area was weak. On the other hand, for the nonstoichiometric surfaces, i.e. Zr-terminated ZrO_2 surface, the bond breaking of the CNT with (3,0) was occurred and it shows the strong diameter dependence. The small diameter CNT has a strong interaction with the nonstoichiometric surfaces, caused by the opening of CNTs and the successive geometrical transform into an arch-like structure. This behavior means that the nonstoichiometric surfaces has a catalytic effect and the activation energy barrier for dissociation of C-C bonds would be very small.

Our results provided an explanation of the variety of CNT-composite fracture toughness by categorizing the types of interactions that occured at the interface between CNTs with SiC(0001), ZrO_2(111), and Al_2O_3(0001) surfaces. The interfacial interaction between CNTs and ceramic surfaces has the mixed covalent-ionic nature which is quantitatively measured by the ICOHP and Bader analyses. The decrease in fracture toughness of CNT-ZrO_2 composite is due to the relatively smaller covalent bond characteristic and also to the larger ionic bond compared to CNT- C-terminated SiC(0001) surface and CNT- O-terminated Al_2O_3(0001) surface.

References

1. C.N.R. Rao, B.C. Satishkumar, A. Govindaraj, Chem. Comm. 2 (16), 1581e1582 (1997).
2. Javey, H. Kim, M. Brink, Q. Wang, A. Ural, J. Guo, P. McIntyre, P. McEuen, M. Lundstrom, and H. Dai, Nat. Mater. 1, 241 (2002).
3. Y. Shan, L. Gao, Nano., 16, 625−630 (2005)
4. Z.Sun , X. Zhang , Na , Z. Liu , B. Han , and G. An,. J. Phys. Chem. B, 110 (27), pp 13410–13414 (2006)
5. A. Kasperski, A. Weibeln , D. Alkattan, C. Estournès, Ch. Laurent, A. Peigney. Ceram. Intl. 41 (2015) 13731–13738.
6. X. Xia, R.J. Oldmana and C.R.A Catlowa, J. Mater. Chem., 21, 14549-14558 (2011)
7. R. Grau-Crespo, N.C. Hernández, J.F. Sanz, and N.H. de Leeuw, J. Phys. Chem. C, 111, 10448-10454 (2007).
8. L. Offernes, P. Ravindran, A. Kajekshus. J. Alloys Comp., Vol. 439 37-54 (2007)
9. M. David, T. Kishi, M. Kisaku, H. Nakanishi and H. Kasai, Jap. J. App. Phys. Vol. 45, No. 4A, (2006). 2869–2871
10. C. Hwua and Y. Yeh, Proc.Struc. Int. 2, 1327–13 (2016).
11. S.M. Dong, Y. Katoh, A. Kohyama, S.T. Schwab, and L.L. Snead,. Ceram. Intl., 28, 899–905 (2002).
12. I. D Aditya, D. Matsunaka, Y. Shibutani, Suprijadi, AIP Adv. (2018) Under reviewing process

Chapter 7 Summary and Future Works

7.1. Summary

In this study, we investigated the interfacial interaction of CNT and ceramic surfaces using first-principles calculations. It has been found that on the stoichiometric ceramic surfaces, namely the Al-terminated Al_2O_3 and O-terminated ZrO_2(111), the structures of all the CNTs did not drastically change from those before adsorbing and the adhesive energy was weak. On the other hand, on the nonstoichiometric surfaces, i.e. O-terminated Al_2O_3, Si- and C- terminated SiC and Zr-terminated ZrO_2 surface, the structure of all the CNTs changed depending on the diameter. This structure change indicates a strong interaction between CNTs and ceramic surfaces. Adhesive energies as a function of diameter of CNTs support the results by Ying Sun and Chena. The small diameter CNT has strong interaction with the nonstoichiometric surfaces, caused by the opening of the CNTs and the successive geometrical transformation into an arch-

like structure. This behavior means that the nonstoichiometric surfaces has a catalytic effect and the activation energy for dissociation of C-C bonds would be very small. The strong interfacial interaction of small diameter CNTs with the nonstoichiometric surfaces would be a possible mechanism for the successful ceramic composite reinforced with CNTs.

Fracture toughness, which is most expected to be improved by adding the CNT into ceramic matrix, also depends on the interface property. The strong interface can resist the crack propagation which might be dependent on the adhesive energy and also the covalent/ionic character of the interface. The strong covalent force between CNTs and O-terminated Al_2O_3(0001) surface is likely to result in the substantial increase in fracture toughness of CNT-Al_2O_3 composites. The fracture toughness CNT-SiC composite is slightly improved because the covalent character is lower than the case of CNT and O-terminated Al_2O_3(0001). And the decrease in fracture toughness of CNT-ZrO_2 composite is due to the relatively smaller covalent bond characteristic and also to the larger ionic bond.

7.2. Future Works

For the future works, we have to challenge the problem on how to lead the macroscopic properties using our current results and method. As of the fracture toughness which is the most important mechanical property in ceramics, we try to classify the types of bonding characterization according to the adhesive energy and the covalent/ionic character consideration. Especially, the point is how the latter result affects the crack propagation behaviors of deflection at the interface or direct propagation over the interface. This challengeable topics would show good fracture

resistance and enhance the mechanical property to be generated when the ceramics are combined with CNTs.

Appendix A

Density Functional Theory

First-principle method (Ab-initio) is a method of calculating atomic and molecular structure directly from the first principles of quantum mechanics, without using quantities derived from experiment as parameters. It can be used, for example, to determine the electronic, magnetic, and mechanics properties of materials or molecules by calculating the total energy of the molecule for a variety of molecular geometries and finding which conformation has the lowest energy.

The central theme of ab initio methods is to obtain accurate solutions to the Schrödinger equation. In general, the state of a particle is defined by a wave function ψ based on the well-known wave-particle duality. The Schrödinger equation is

$$\left[\frac{h^2}{2m}\sum_{i=1}^{N}\nabla_i^2+\sum_{i=1}^{N}V(\vec{r}_i)+\sum_{i=1}^{N}\sum_{j<1}U(\vec{r}_i,\vec{r}_j)\right]\psi=E\psi \qquad (1)$$

Here, m is the electron mass, $\sum_{i=1}^{N}\nabla_i^2$, $\sum_{i=1}^{N}V(\overrightarrow{r_i})$, $\sum_{i=1}^{N}\sum_{j<1}U(\vec{r}_i,\vec{r}_j)$ define the kinetic energy of each electron, the interaction energy between each electron and the collection of atomic nuclei, and the interaction between different electrons respectively, ψ is the electronic wave function which is a function of each spasial coordinates of each of N electrons, so $\psi=\psi(\vec{r}_i....,\vec{r}_N)$, and E is the ground state energy of the electrons.

Some approximations such as the density functional approach are used to solve time consuming problem of the pristine ab initio method. The density functional theory

(DFT) is based on the fact that the ground-state electronic energy is a unique functional of the electronic density $\rho(\vec{r})$, instead of many-body interacting wave functions. The electron denstity can be written in terms of the individual electron wave function as:

$$\rho(\vec{r}) = 2\sum_i \Psi_i^*(\vec{r})\Psi_i(\vec{r}) \tag{2}$$

Here, the summation goes over all the individual electron wave function that are occupied by electrons, so the term inside the summation is the probability that an electron in individual wave function $i(\vec{r})$is located at position $\vec{r}$. Due to the electron spin and Pauli exclusion principle states electrons provided they have different spins, the factor 2 appears in front of the summation. The electron density $\rho(\vec{r})$, is the source of information that we need and actually physically observable from the full wave function solution to the Schrödinger equation, which is a function of *3N* coordinates.

By introducing the variational principle, we obtain a one-electron Schrödinger equation (also called the Kohn–Sham equation) for the Kohn–Sham wavefunction [(22)]

$$\left[-\frac{\hbar^2}{2m}\sum_{i=1}^{N}\nabla_i^2 + V(\vec{r}) + V_H(\vec{r}) + V_{XC}(\vec{r})\right]\psi_i(\vec{r}) = \in_i \psi_i(\vec{r}) \tag{3}$$

These equations are similiar with the Schrödinger equation. The main difference is the summation in the full Schrödinger equation is not appear in the Kohn-Sham equations. This is because the solution of the Kohn- Sham equations are single-electron wave function that depend on only three spasial variables, $i(\vec{r})$. There are three potential in the Kohn Sham equations.

The *V* is the potential defines the interaction between an electron to the collection of atomic nuclei. The V_H is called the Hartree potential and is defined as:

$$V_H(\vec{r}) = e^2 \int \frac{\rho(\vec{r}')}{|\vec{r} - \vec{r}'|} d^3 r'$$

Hartree potential describes the Coulomb potential between the electron being considered in one of the Kohn-Sham equations and the total electron density defined by all electrons in the problem. Finally, the V_{XC} can formally be defined as a functional derivative of the exchange-correlation energy:

$$V_{XC} = \frac{\delta E_{XC}[\rho(\vec{r})]}{\delta \rho(\vec{r})}$$

Finally, the algorithm of DFT is an iterative way as outlined below :

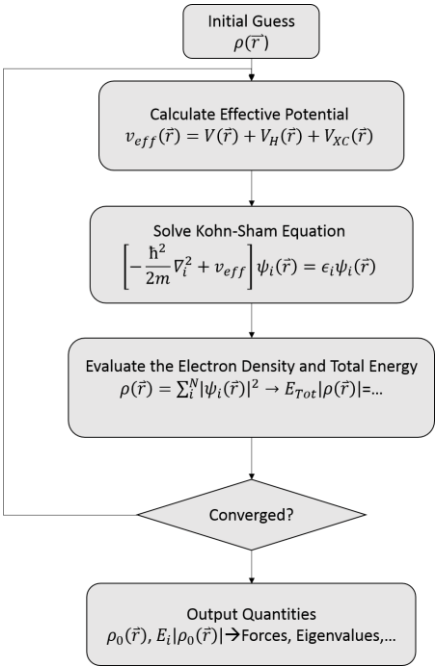

FIG.A. 1. A flow chart of the DFT iteration scheme

Appendix B

Crystal Orbital Hamilton Populations and Bader Analysis

Crystal Orbital Hamilton Populations (COHP)[1]

To determine the nature of bonding in a given solid-state material, it is necessary to extract the chemical bonding information from the electronic band structure that is computed for the respective material by using a quantum-mechanical technique. the total energy of a many-particle system, i.e., the sum of the potential and kinetic energy, needs to be calculated solving the time-independent Schrödinger equation.

Let us looking at the example below :

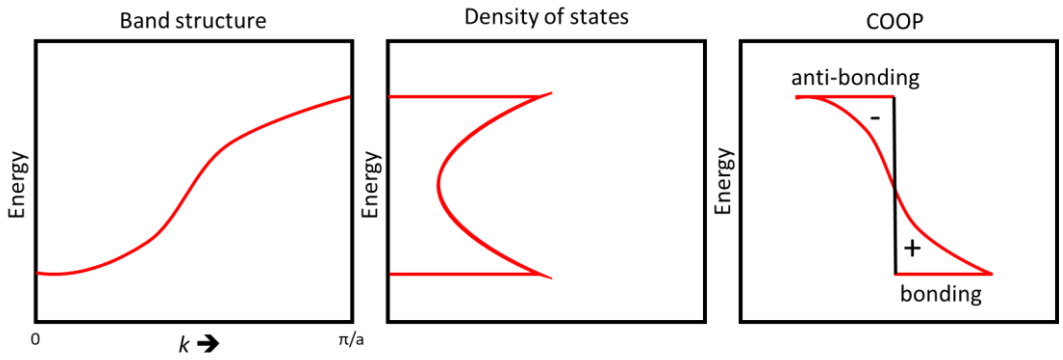

(a) (b) (c)

FIG. B.1 Simple “one dimensional” (a) band structure, (b) DOS, (c) COOP curve

The density-of-states (DOS) diagram in the middle results as the inverse slope of the band structure on the left. A bonding indicator for the solid can be easily constructed by generating an overlap population-weighted density-of-states, the crystal orbital overlap population (COOP), given on the right part of the above figure.

The COOP results from multiplying the DOS by the overlap population, and it adds an additional dimension—the bonding information: it adopts positive values (bonding, because of the positive overlap population) and negative values (which identify antibonding interactions). By comparing the band structure and its orbital icons with the COOP diagram, it is obvious why the nearest-neighbor COOP is bonding at low energies and antibonding at high energies.

If one can weight the DOS by the overlap population, one can also weight it by the corresponding element of the Hamiltonian. In fact, technical reasons arising within density-functional techniques suggest to choose the latter method, dubbed Link crystal orbital Hamilton population (COHP). By doing so, we partition the band structure energy (instead of the electrons) but again into bonding, nonbonding, and antibonding contributions.

The crystal orbital Hamiltonian population density (COHP) measures the magnitude and sign of the bond order energy overlap between atomic orbitals located on different atoms. This enables the determination of the bonding versus the antibonding nature of orbital fragments. It is also a measure of the interaction strength between two atomic orbitals.

$$\begin{aligned} -COHP_{ij}(E) &= H_{ij}P_{ij}(E) \\ &= H_{ij}\sum_{n} c_i^n c_j^n \delta\left(E - E_n\right) \end{aligned} \tag{1}$$

$$\begin{aligned} ICOHP &= \int_{-\infty}^{E_F} dE \sum_{i,j} COHP_{ij}(E) \\ &= \frac{1}{2}\sum_{N_i}^{occ} N_i E_i \end{aligned} \tag{2}$$

Where N_i is electron occupation of the molecular orbital and E_n represents the Kohn–Sham orbital energies. H_{ij} is the plane wave Hamiltonian and density-matrix element P_{ij}. The coefficient c_i^n is related to the molecular orbital :

$$\Psi_n = \sum_i c_i^n \varphi_i \tag{3}$$

Where φ_i denotes atomic orbital. The integrated ICOHP value can be considered as a measure of the bond strength. It is not an exact expression for the bond energy, but a good approximation as long as the repulsive energy of the nuclei cancels out the double counted electrostatic interactions.[2] ICOHP is the maximum for a covalent bond when all bonding orbitals are occupied by electrons and none for the antibonding orbitals. In order to make COHP plots look similar to COOP, we can plot –COHP diagrams so that bonding states (positive) and antibonding states (negative) and it is easier to interpret.

Bader Decomposition of Charge Density[3]

The properties of chemicals and materials are often described in terms of charge transfer between atoms and the presence of ionic charges. This also indicating the ionic bonding between atoms. One way to approach this is by using charge density as has been proposed by Bader[4]. Space is then divided into regions by surfaces that run through minima in the charge density.

The charge density in molecular system reaches a minimum between atoms and this is a natural place to separate atoms from each other. Bader divided surface into what so called *bader region.* Bader region uses what zero flux surfaces which is 2-D surface on which the charge density is a minimum perpendicular to the surface to divide atoms.

More precisely, at a point on a dividing surface the gradient of the electron density has no component normal to the surface.

Each Bader region often contains one nucleus, sometimes no nucleus is found within a Bader region. By integrating the electronic density within the Bader region where an atom's nucleus is located, and possibly adding the electronic charge in nearby regions that do not include a nucleus, the total charge on an atom can be estimated.

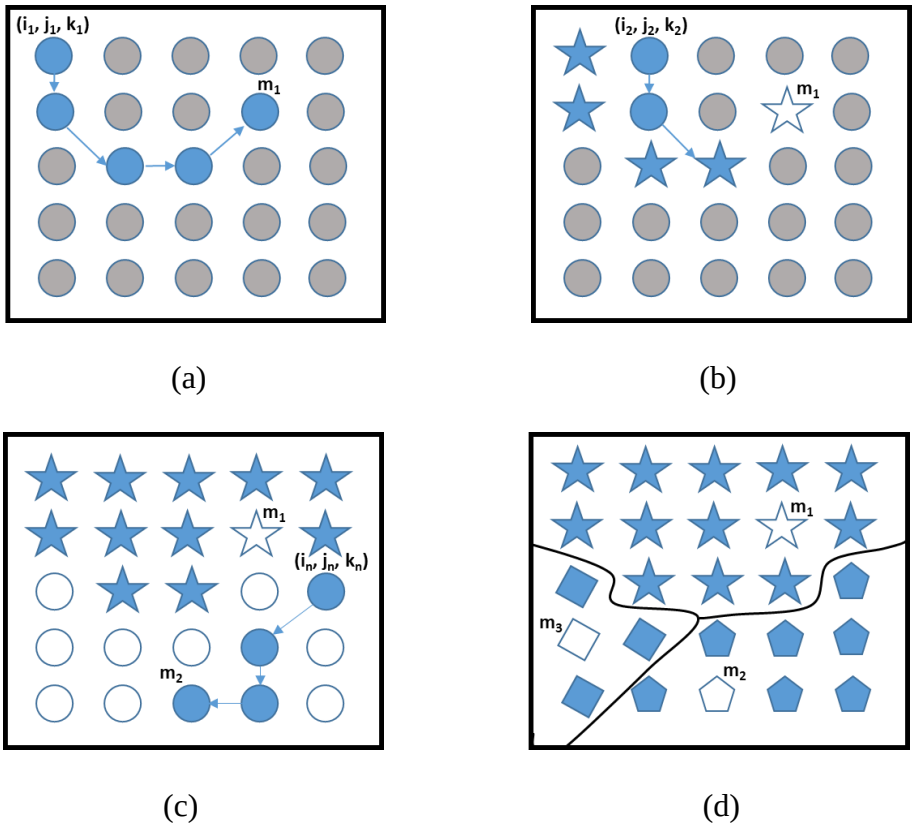

FIG. B.2. An illustration of the steepest ascent paths (a) the set of points which terminate at maximum m_1, (b) the set of points which terminate at grid point in Bader region 1. (c), the set of points which terminate at maximum m_2 constitute that Bader volume. (d) The Bader surfaces (black line) separate the volumes. These ascent trajectories are constrained to the grid points, moving at each step to the neighboring grid point towards which the charge density gradient is maximized. Each trajectory either terminates at a new charge density maximum, m_n , or at a grid point which has already been assigned.

FIG. B.2 shows the computational method for partitioning a charge density grid into Bader volumes which is efficient, robust, and scales linearly with the number of grid points. To simplify the algorithm, we assume the charge density grid points to form an orthogonal lattice. This algorithm essentially looks for maximum charge density by following the density gradient ascent trail from one grid point to another grid point. When the algorithm provides grid points to fill the density limit, the path is then terminated when they reach the predefined grid point. In order to associate each grid point with a Bader region, a path of steepest ascent in the charge density is found.

More specifically, a steepest ascent move from a grid point (*i*,*j*,*k*), is made along the direction which maximizes the charge density gradient, $\nabla\rho$, is calculated along the 26 possible directions, $\hat{r}$, towards adjacent grid points, using

$$\nabla\rho(i,\ j,k)\bullet\hat{r}(di,dj,dk)=\frac{\Delta\rho}{|\Delta\vec{r}|}$$

Where di,dj,dk are each assigned the values $\{-1,0,1\}$ but excluding $di=dj=dk=0$. The change in density

$$\Delta\rho=\rho(i+di,\ j+dj,k+dk)-\rho(i,\ j,k)$$

and the distance

$$|\Delta\vec{r}|=|\vec{r}(i+di,\ j+dj,k+dk)-\vec{r}(i,\ j,k)|$$

are evaluated between neighbors of each points, where $\vec{r}(i,\ j,k)$is the Cartesian vector to the grid point (*i*,*j*,*k*). The steepest ascent step selected, $\vec{r}(di,dj,dk)$, is the one that maximizes the positive values of $\nabla\rho(i,\ j,k)$. If there are no positive values, the point (*i*,*j*,*k*) is considered to be a charge density maximum.

Lets take a look at Fig. B.2 (a) that illustrates the algorithm. (i_1,j_1,k_1) was choosen as our computational starting point. We found charge density maximum m_1 by following a steepest ascent path. The number assigned to the maximum (1 in this case)

is entered in an array for each point along the trajectory. In this way, each of the points along the path is assigned to Bader region 1. A steepest ascent path from each one of these points terminates at m_1. Then, we pick the point (i_2,j_2,k_2) that has not already been assigned as our starting point for a new steepest ascent path. The path is extend until it reaches new maximum charge density or grid point. In Fig. B.2 (b), the second path reaches a point known to be in Bader region 1 after just two ascent steps, allowing the path to be terminated early. Each point along the ascent path from (i_2,j_2,k_2) is then assigned to the region corresponding to m_1.

A new entry are made in the list of known charge density maxima and the points along the ascent path are given the value 2. When an ascent path start from a point (i_n,j_n,k_n) this path reaches a maximum at point m_2, as shown in Fig. B.2 (c), a new entry is made in the list of known charge density maxima and the points along the ascent path are given the value 2. When a steepest ascent trajectory has been initiated from all grid points, the partitioning analysis is complete, and all grid points have then been assigned to a Bader region. For further analysis, for example, calculations of charge density differences, the assignment of the grid points to Bader regions is all that needed. The computational effort, therefore, scales linearly with the number of grid points and is independent of the number of atoms in the system.

References

1. R. Dronskowski and P. E. Bloechl, , J.Phys.Chem., 97, (1993) 8617–8624.

2. G.A. Landrum and R. Dronskowski, Angew. Chem., Int. Ed., 39, (2000) 1560–1585.

3.G. Henkelman, A. Arnaldsson, H. Jónsson., Comp. Mat. Sci. 36, 3, (2006) 354-360

4. R. Bader., Oxford University Press, New York (1990).

Appendix C

Supported Data and Preliminary Calculation

Average CNTs C-C Covalent Bonding

Besides using cohesive energy, the strength of the C-C bond is also evaluated through the ICOHP value which is also used to measure the strength of the covalent bond on the interface between the CNT and the ceramic. In the freestanding condition, the –ICOHP value of the CNTs are as follow :

Table C.1. Average C-C bond ICOHP values of CNTs and Graphene

CNT	Average ICOHP (eV)
(3,0)	-9.1515
(6,0)	-9.97064
(9,0)	-10.3081
(12,0)	-10.5646
Graphene	-11.04727

The C-C bond become stronger when the CNT diameter increase. This result is in accordance to our cohesive energy data depicted in the Chapter 2.

Graphene-O-terminated Al_2O_3

As our first step, we calculate the graphene and O-terminated Al_2O_3 system as as has been done by Etani et. al.[1] They observe the distance between graphene and O-terminated Al_2O_3 surface using normal-incidence X-ray standing wave (NIXSW) spectroscopy and calculate DFT.

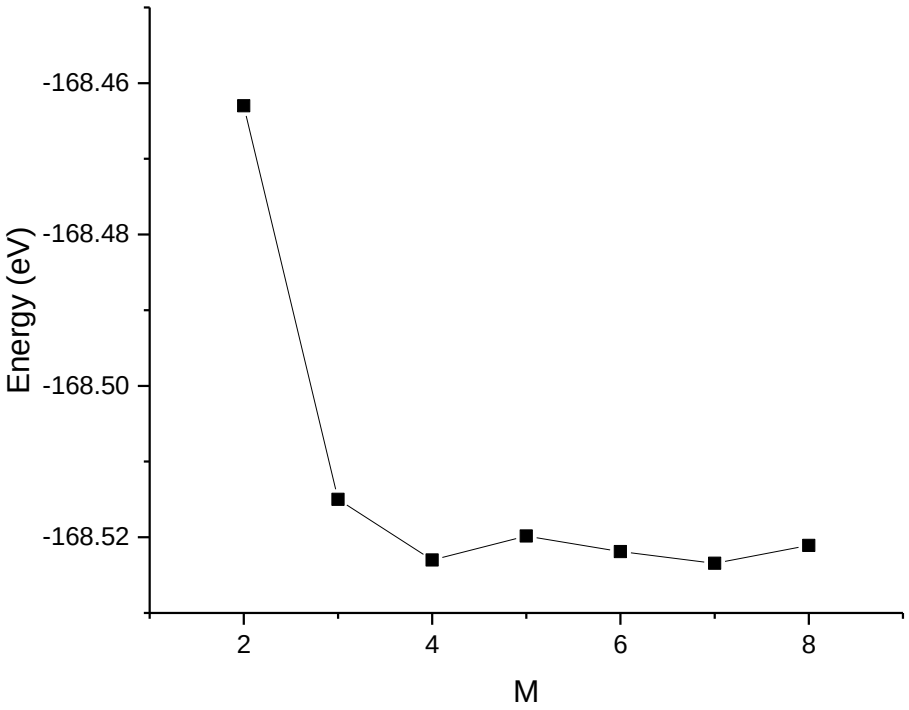

FIG. C.1. **k**-point convergence result

To determine the **k**-point used in this work, we perform convergence test using graphene-Al_2O_3 system with different M value for a M×M×1 Monkhorst-Pack mesh[2]. This system was chosen because of the availability of reference both DFT and

experimental calculations perform by Etani et al[1]. After that, we calculate our model using parameter that has been mention in the chapter 2.

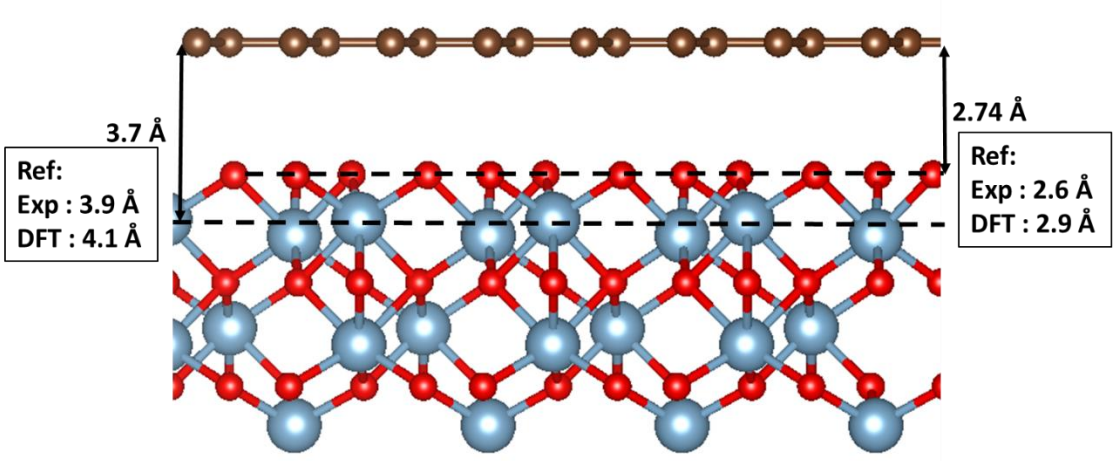

FIG. C.2. Atomic structure between the graphene and Al_2O_3 (0001)

As can be seen in the FIG. C.2 that our result are in very good agreement with the reference result. The van der walls correction play important role in calculating the distance between graphene and O-terminated α-Al_2O_3(0001). Before using vdW correction, the distance between graphene and O-terminated α-Al_2O_3(0001) surface is 3.5Å. vdW helps to correct the distance between graphene and O-terminated α-Al_2O_3(0001). Without using this correction, the distance between graphene and Al_2O_3 would be much larger than it should be.

The electrostatic interactions between graphene and α-Al_2O_3(0001) for can be understood form Fig. C.3, which shows the partial densities of states of graphene and α-Al_2O_3(0001).

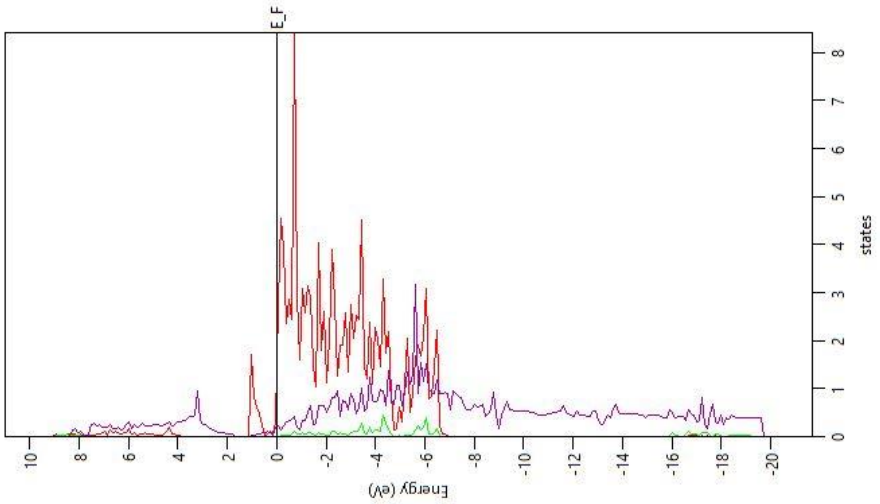

FIG. C.3 Partial density of states of *pz* orbitals of graphene (in purple), the first Al layer (in green) and the topmost O layer, which is decomposed into *p* orbitals (in red), for graphene/O-terminated Al_2O_3(0001).

In graphene/α-Al_2O_3(0001), the Dirac point of graphene is shifted to 1.1-1.3 eV relative to the freestanding case . This result in good agreement with the reference. After obtaining the appropriate calculation parameters, then the calculation is continued by combining the CNT with ceramic surface that is Al_2O_3 (0001), SiC (0001), and ZrO_2 (111) using static calculations.

Optimize position of CNTs on ceramic surfaces

To obtain an appropriate result, we analyze some possible positions where CNTs can be placed on the ceramic surface and compare the energy of the CNT / ceramic in each of those positions. Here are the energy of each position :

CNT/Al-terminated Al_2O_3 (0001)

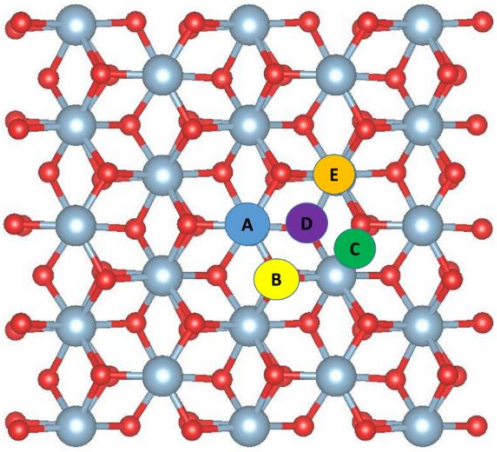

FIG. C.4 CNT sites at Al-terminated Al_2O_3 (0001)

Table C.2. Energy of CNT/Al-terminated Al_2O_3 (0001) in several positions

CNT	Energy at Site Position (eV)				
	A	B	C	D	E
(3,0)	-524.6589	-524.59382	-524.57041	-524.4713	-524.66139
(6,0)	-642.92859	-642.90267	-642.91937	-640.6789	-639.52595
(9,0)	-753.49071	-753.63489	-753.64213	-753.1290	-753.65158
(12,0)	-852.71964	-852.7294	-852.69241	-852.4623	-852.75874

CNT/O-terminated Al_2O_3 (0001)

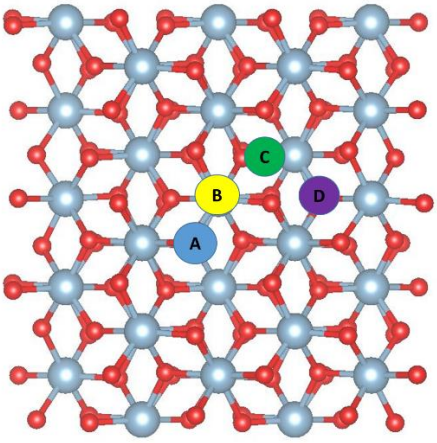

FIG. C.5 CNT sites at O-terminated Al_2O_3 (0001)

Table C.3. Energy of CNT/O-terminated Al_2O_3 (0001) in several positions

CNT	Energy at Site Position (eV)			
	A	B	C	D
(3,0)	-574.77712	-574.41057	-574.53817	-572.16792
(6,0)	-687.52245	-686.35546	-687.3543	-685.9049
(9,0)	-797.75231	-797.08211	-797.63845	-796.84851
(12,0)	-897.03061	-896.82634	-897.00042	-896.3243

Optimize position of CNTs on SiC (0001)

CNT/Si-terminated SiC (0001)

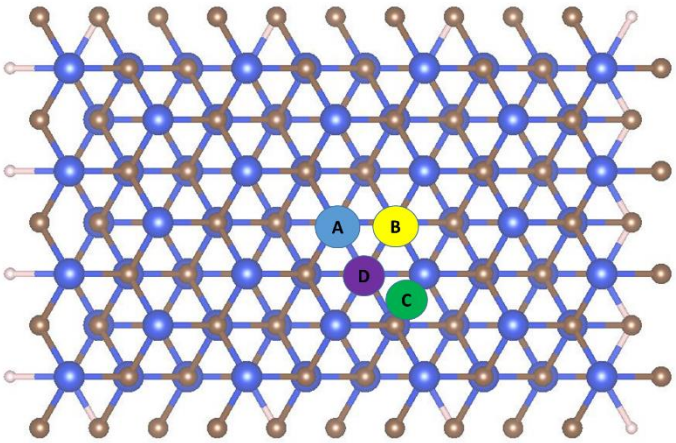

FIG. C.6 CNT sites at Si-terminated SiC (0001)

Table C.4. Energy of CNT/Si-terminate`d SiC (0001) in several positions

CNT	Energy at Site Position (eV)			
	A	B	C	D
(3,0)	-1138.8949	-1139.0572	-1139.4166	-1139.4793
(6,0)	-1366.246	-1365.5656	-1325.5622	-1365.4107
(9,0)	-1548.8815	-1520.1332	-1518.5523	-1547.5784
(12,0)	-1811.1839	-1811.1237	-1811.3002	-1811.3758

CNT/C-terminated SiC (0001)

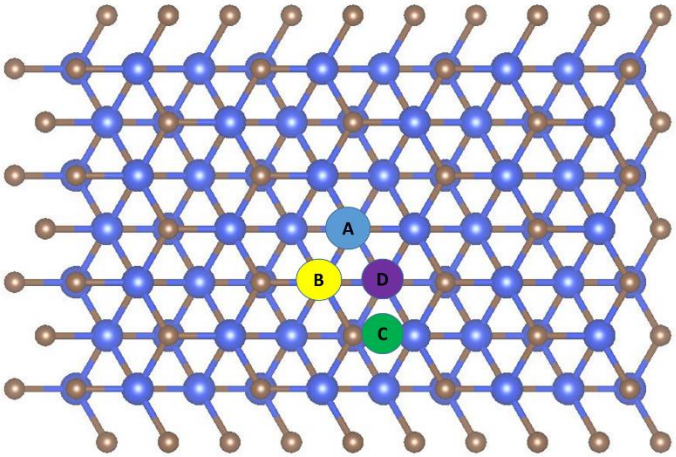

FIG. C.7 CNT sites at C-terminated SiC (0001)

Table C.5. Energy of CNT/C-terminated SiC (0001) in several positions

CNT	Energy at Site Position (eV)			
	A	B	C	D
(3,0)	-1132.9585	-1131.9697	-1133.8032	-1130.4148
(6,0)	-1361.6219	-1361.2066	-1361.5412	-1360.8649
(9,0)	-1585.3129	-1585.3184	-1585.2528	-1585.2528
(12,0)	-1807.3023	-1807.1552	-1807.1374	-1807.1494

CNT/Zr-terminated ZrO_2 (111)

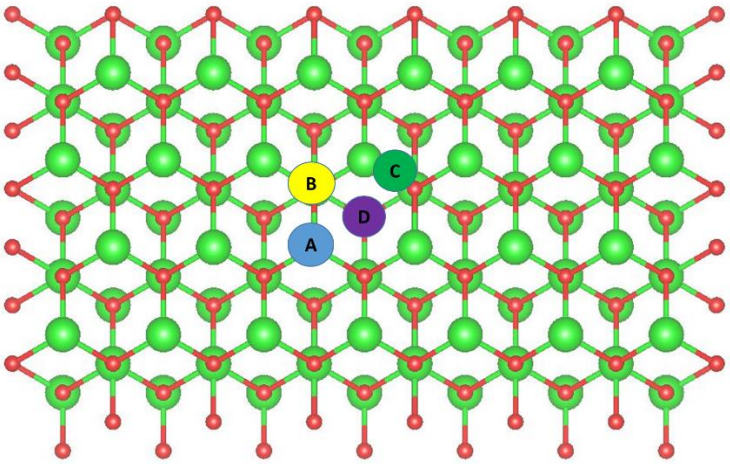

FIG. C.8 CNT sites at Zr-terminated ZrO_2 (111)

Table C.6. Energy of CNT/Zr-terminated ZrO_2 (111) in several positions

CNT	Energy at Site Position (eV)			
	A	B	C	D
(3,0)	-1836.1264	-1836.53	-1838.0474	-1837.6504
(6,0)	-2181.3802	-2181.0658	-2182.1576	-2181.3757
(9,0)	-2521.6114	-2522.6269	-2522.0058	-2521.6039
(12,0)	-2858.14	-2857.9639	-2858.7353	-2858.1412

CNT/O-terminated ZrO_2 (111)

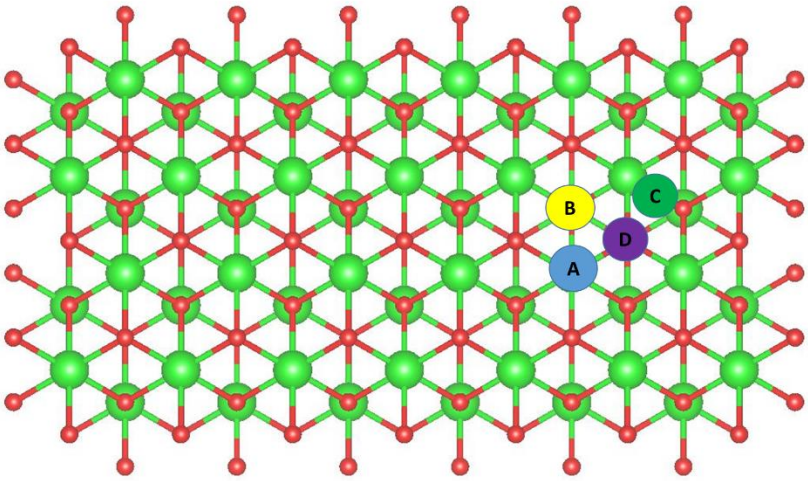

FIG. C.9 CNT sites at O-terminated ZrO_2 (111)

Table C.6. Energy of CNT/O-terminated ZrO_2 (111) in several positions

CNT	Energy at Site Position (eV)			
	A	B	C	D
(3,0)	-1656.4006	-1656.3206	-1656.3479	-1656.3548
(6,0)	-2006.6827	-2006.6719	-2006.6666	-2006.6723
(9,0)	-2345.7037	-2345.7027	-2349.5614	-2345.7045
(12,0)	-2683.2729	-2683.2638	-2683.2606	-2683.2705

The results shown in Chapters 4-6 are the selected structures based on the above calculations where the selected position is a position that has a more negative value

which means it has a more optimum position. We then relax the structure in the predetermined position of the calculation until it reaches the most optimize structure as shown in chapter 4-6.

After interact with ceramic surfaces, some CNTs change it structure especially for the small diameter CNT. The average covalent bond (ICOHP) between the C atoms on CNTs also changes in value as follows:

At its optimum position, the carbon atoms of the CNT will bind to the atoms on the ceramic surface. The bond, as discussed in chapter 4-6, is a mixture of covalent and ionic bonds. The covalent bonds are diverse and can be demonstrated from the following values of ICOHP:

Table C.7. ICOHP of C atom/s of CNTs and Interacted atoms of ceramic surfaces.

CNT	Al_2O_3		SiC		ZrO_2	
	Al terminated	O terminated	Si terminated	C terminated	Zr terminated	O terminated
	ICOHP	ICOHP	ICOHP	ICOHP	ICOHP	ICOHP
(3,0)	-3.54	-7.28 - -15.72	-5.04 - -5.89	-5.01 - -9.84	-1.04 - -2.23	-10.26 - -10.86
(6,0)	-1.93	-14.60 - -15.56	-4.29 - -5.55	-7.65 - -8.58	-0.98 - -1.97	-0.08
(9,0)	-0.82	-8.27 - -11.93	-4.11 - -5.58	-7.41	-0.83 - -0.91	-0.06
(12,0)	-0.7	-7.65 - -11.71	-2.88 - -4.86	-7.24	-0.85 - -1.39	>-0.03
Graphene	-0.02- -0.05	-0.014	-0.13 - -4.65	-0.16	-0.5 - -1.4	-0.01

The above results indicate that the ICOHP value decreases as the CNT diameter increases. Total ICOHP on the interaction of CNTs with ceramic surfaces shown in chapter 4-6 is the sum of each covalent bond whose range is shown in the above table. After interacting with the ceramic surface the structure of the CNTs is changed, especially when interacting with non stoichiometric surfaces. Therefore, the covalent

bonds of the CNT will also change. We calculate the strength of the bond by using -ICOHP as shown in the following table:

Table C.8. Average ICOHP of C-C bonds of the CNTs after interacting with ceramic surfaces.

CNT	Al_2O_3		SiC		ZrO_2	
	Al terminated	O terminated	Si terminated	C terminated	Zr terminated	O terminated
	Avg CNTs ICOHP	Avg CNTs ICOHP	Avg CNTs ICOHP	Avg CNTs ICOHP	Avg CNTs ICOHP	Avg CNTs ICOHP
(3,0)	-9.39	-10.43	-9.23	-9.81	-9.39	-9.17
(6,0)	-9.84	-10.64	-9.26	-9.54	-9.68	-9.95
(9,0)	-9.87	-10.89	-9.54	-9.96	-10.04	-10.09
(12,0)	-10.05	-11.02	-9.61	-10.03	-10.14	-10.18
Graphene	-10.89	-11.04	-10.56	-10.23	-10.88	-11.03

The data in the table above shows that although the CNT structure changes (there is a broken C-C bond) does not necessarily make the mechanical properties of the CNTs weaker. In fact, for the smallest diameter CNT, the C-C bonds become stronger after interact with ceramic surfaces.

References

1. S. Entani, L.Y. Antipina, P.V Avramov, et al. Nano Res. 8: 1535 (2015).
2. H. J. Monkhorst, J. D. Pack, Phys. Rev. B 13, 5188 (1976).

Acknowledgements

All praises to Allah SWT, the Most Gracious and the Most Merciful, and and may His peace and blessings be upon the Prophet. I would like to express my deep gratitude to Professor Yoji Shibutani and Professor Daisuke Matsunaka, my research supervisors, for their patient guidance, enthusiastic encouragement and useful critiques of this research work. As my teacher and mentor, they has taught me more than I could ever give him credit for here. They has shown me, by their example, what a good Scientist (and person) should be. And also Professor Suprijadi, Dr. Widayani, and Dr. Nugraha as a supervisors in ITB which always gives encouragement and useful input. I also like to thanks to collaborator of these research works: Prof. Go Yamamoto for giving us the idea of this research. I would also thank Professor Yoshitada Morikawa, Professor Kazunori Sato, Professor Wilson Agerico Dino, as my thesis examiners, which gives critiques and useful input.

I would also like to thanks to the Ministry of Research, Technology and Higher Education of the Republic of Indonesia for the scholarship during the doctoral course in Osaka University.

Nobody has been more important to me in the pursuit of this degree than the members of my family. I would like to thank my parents, whose love and guidance are with me in whatever I pursue. They are the ultimate role models. Most importantly, I wish to

thank my loving and supportive wife, Annisa Erliana Devyanti, and my daughter, Kimiko Hava Tavisha, who provide unending inspiration.

List of Publication

I. D Aditya ,. D. Matsunaka, Y. Shibutani, G. Yamamoto, "*First-principles Study of Interfacial Interaction Between Carbon Nanotube and Al_2O_3(0001)*", Journal of Applied Physics **121**, 025304 (2017)

I. D Aditya, D. Matsunaka, Y. Shibutani, Suprijadi, "*First-principles Study of Interfacial Interaction between Carbon Nanotube and Stoichio- and Nonstoichiometric Ceramic Surfaces*", accepted to Materials Transactions.

List of Presentations

I.D. Aditya , D. Matsunaka, Y. Shibutani, G. Yamamoto International Workshop on Advanced Materials and Nanotechnology 2016 (IWAMN 2016)-Hanoi, November 5th 2016

I.D. Aditya , D. Matsunaka, Y. Shibutani, *The International Conference on Computation in Science and Engineering (ICCSE 2017)- Bandung, July 10-12th 2017*

I.D. Aditya , D. Matsunaka, Y. Shibutani. *International Symposium on Nanoscience and Nanotechnology In Life Science November 28-29th 2017*

I.D. Aditya , D. Matsunaka, Y. Shibutani. *International Symposium on Computational Science- Bandung, May 8-9th 2018*